LiDAR Individual Tree Detection for Assessing Structurally Diverse Forest Landscapes

Sean Jeronimo

A thesis

submitted in partial fulfillment of the

requirements for the degree of

Master of Science

University of Washington

2015

Committee:

Jerry F. Franklin, Chair

Gregory J. Ettl

Robert J. McGaughey

Van R. Kane

Program Authorized to Offer Degree:

School of Environmental and Forest Sciences

University of Washington

Abstract

LiDAR Individual Tree Detection for Assessing Structurally Diverse Forest Landscapes

Sean Jeronimo

Chair of the Supervisory Committee:
Professor Jerry F. Franklin
School of Environmental and Forest Sciences

Contemporary forest management on public land incorporates a focus on restoration and maintenance of ecological functions through silvicultural manipulation of forest structure on a landscape scale. Incorporating reference conditions into restoration treatment planning and monitoring can improve treatment efficacy, but the typical ground-based methods of quantifying reference condition data – and comparing it to pre- and post-treatment stands – are expensive, time-consuming, and limited in scale. Airborne LiDAR may be part of the solution to this problem, since LiDAR acquisitions have both broad coverage and high resolution. I evaluated the ability of LiDAR Individual Tree Detection (ITD) to describe forest structure across a structurally variable landscape in support of large-scale forest restoration. I installed nineteen

0.25 ha stem map plots across a range of structural conditions in potential reference areas (Yosemite National Park) and potential restoration treatment areas (Sierra National Forest) in the Sierra Nevada of California. I used the plots to evaluate a common ITD algorithm, the watershed transform, compare it to past uses of ITD, and determine which aspects of forest structure contributed to errors in ITD. I found that ITD across this structurally diverse landscape was generally less accurate than across the smaller and less diverse areas over which it has previously been studied. However, the pattern of tree recognition is consistent: regardless of forest structure, canopy dominants are almost always detected and relatively shorter trees are almost never detected. Correspondingly, metrics dominated by large trees, such as biomass, basal area, and spatial heterogeneity, can be measured using ITD, while metrics dominated by smaller trees, such as stand density, cannot. Bearing these limitations in mind, ITD can be a powerful tool for describing forest structure across heterogeneous landscape restoration project areas.

Table of Contents

List of Tables

List of Figures

Acknowledgements

First and foremost, I would like to thank – in chronological order – my parents, the late Peter McDonald, and Jerry Franklin for kindling my love of and interest in the natural world, forestry, and forest science. Without the encouragement of James Freund and Jim Lutz I would never have made good on this interest, and I thank them for encouraging me to make the leap from the world of 1s and 0s to the world of DBH and for providing me with foundational field experience. Since making the leap, Derek Churchill has provided constant support in terms of learning and work opportunities, and I value the partnership and friendship that we have built very much. I would not be doing the work that I do today without Derek. My committee members – Jerry Franklin, Greg Ettl, Bob McGaughey, and especially Van Kane – have done the indispensable work of reining me in when my research started to wander, and in doing so have taught me many important lessons about how to carry out a research project. I would also like to thank my field crew, Luke Dow and Caileigh Shoot, for their uncomplaining hard work and ready willingness to carry lots of heavy gear. Lastly, I thank my partner Melissa Pingree for her love and support, which I could not do without.

This work was supported by the USDA Forest Service Pacific Southwest Research Station through grants 14-JV-11272139-014, “Using LiDAR to Guide Restoration in Sierra Nevada Forests”, and 13-CS-11052007-055, “Using Light Detection and Ranging (LiDAR) to Guide Burned Landscape Recovery and Restoration in Sierra Nevada Forests.”

Introduction

Objectives for management of forest ecosystems on public land are often defined in terms of desired ecosystem functions, such as disturbance resistance and resilience, habitat provision, and hydraulic regulation (e.g., North et al. 2009; USDA 2013). Much scientific and management effort is currently focused on restoring desired functions over landscapes degraded by active and passive anthropogenic alteration (Hessburg et al. 2005; Peterson et al. 2005). Practically, restoration of function is achieved through silvicultural manipulation of forest structure and composition (Franklin et al. 2013).

To enhance the effectiveness of restoration, many forest managers are developing treatment prescriptions with a basis in reference datasets, which describe ranges of conditions in functionally intact forests (Covington & Moore 1994; Churchill et al. 2013; Underhill et al. 2014; Tuten et al. 2015). The condition of restoration units is evaluated before and after treatment in context of the reference condition envelope, providing managers with a realistic frame of reference for planning and monitoring silvicultural activities (Moore et al. 1999; Churchill et al. 2013). There are several points in this process at which forest structure must be quantified: definition of reference conditions, assessment of current conditions, development of the silvicultural prescription, and monitoring of the eventual treated stand (Figure 1).

Quantification of structure in support of restoration is typically achieved by installing plots to measure composition, density, the spatial pattern of trees, and characteristics of open space in reference areas and treatment units (Franklin et al. 2013; Lydersen et al. 2013; Fry et al. 2014). In order to capture attributes of spatial pattern and open space, these plots are often stem mapped, that is, every tree within the plot is accurately mapped in 2- or 3-dimensional space.

Reference conditions defined from stem map plots are currently being used to inform restoration on 1000s of hectares of federal and state land in Oregon and Washington (e.g., USDA 2013).

Cost – in terms of both time and money – is a major impediment to the collection of stem map data. Typical stem maps for characterization of reference conditions are done on plots between 1 and 4 ha in size (North et al. 2009; Larson & Churchill 2012), and plot replication is usually necessary to capture the range of conditions in a project area. Installing many large plots requires a considerable amount of field time by trained personnel. Efficient and accurate stem map data collection also requires precision surveying equipment, which itself can be a financial burden. Together, these costs can easily overwhelm restoration budgets, which usually rely on marginal receipts from stewardship contracts (Schulz et al. 2012). Because of these impediments, many forest managers who would like to base restoration treatments on reference conditions do not have access to the requisite data.

Another important limitation of stem maps is the practical constraint of scale. Even without considering budget limitations, it would be impractical to install enough stem map plots over a large enough area to allow for spatially explicit landscape evaluation. But restoration of ecosystem functions requires an understanding of ecological processes operating at multiple scales (Franklin et al. 2007; Hessburg et al. 2015), and must include large-scale measures of pattern such as patch size, shape, connectivity, and hierarchy (Kotliar & Wiens 1990; Wu 1999). Clearly, ground-based methods cannot efficiently satisfy the data demands of such involved landscape analyses.

An appealing solution to the problems of cost and scale is the use of airborne LiDAR systems to directly measure forest canopies over large areas of land. Hummel et al. (2011) determined that

the cost of LiDAR inventory is comparable to installing traditional fixed- or variable-radius inventory plots. When stem map data are required the cost of field work is increased substantially while the cost of LiDAR is maintained; accordingly, my informal analyses show that the cost of acquiring LiDAR data can be 2-3 orders of magnitude less than the cost of installing ground-based stem maps. The savings become even more favorable as acquisition area increases, since a portion of the LiDAR expense is due to area-independent mobilization costs (Laes et al. 2008). In many cases, costs of LiDAR acquisition can be shared between several beneficiaries, since, in addition to vegetation inventory, the data can be used for geomorphologic and hydraulic mapping (French 2003), landslide risk assessment (Jaboyedoff et al. 2012), management of archæological amenities (Bewley et al. 2005), and many other applications. The greatest savings, however, are had when LiDAR data are already available, which is increasingly common on public land: many Forest Service districts and National Parks have already invested in the acquisition of LiDAR data over large (10,000s of ha) areas. These data, often originally collected for unrelated purposes, could potentially be used to quantify spatial patterns at little additional cost.

Along with cost savings, LiDAR offers the unique advantage of high resolution data combined with complete coverage over large areas. These attributes make it particularly well-suited for landscape restoration. For one, LiDAR is sure to capture all structural conditions across the acquisition area, even rare conditions that may not be sampled in a randomized plot design. Also, LiDAR allows for analysis at any scale from the individual tree to the entire acquisition, presenting the possibility of truly multi-scale planning and monitoring activities.

In this study, I investigate the application of LiDAR to measuring forest structure in support of silvicultural landscape restoration. In particular, I focus on one family of LiDAR methods: individual tree detection.

Individual tree detection (ITD) refers to partitioning the LiDAR point cloud into segments representing individual trees based on the geometry of the point data (Breidenbach et al. 2010). Typically, the resultant segments are measured (for height, crown diameter, and metrics derived from these) and compiled into a list that is used in much the same way as a field-collected tree list. For instance, ITD data has been used to: estimate standard forest inventory metrics such as density, basal area, or merchantable volume (Bortolot & Wynne 2005; Edson & Wing 2011; Yu et al. 2011); predict ecologically relevant parameters of forest structure such as canopy cover, aboveground biomass, and the spatial pattern of trees (Huang et al. 2009; Tao et al. 2014; Packalen et al. 2013); and assess variables of interest for management such as fire risk (Morsdorf et al. 2004).

Though many studies have sought to perfect ITD algorithms (see Kaartinen et al. 2012 and Vauhkonen et al. 2012 for algorithm reviews), virtually all have come across the same major limitation: the only trees that can be detected reliably are “immediately dominant” trees, that is, those with direct visibility from the air. Richardson & Moskal (2011) suggested that airborne LiDAR is simply incapable of systematically sampling subdominant structures and urge practitioners to be conscious of this limitation when performing analyses. Falkowski et al. (2008) additionally indicate that the potential accuracy of ITD decreases as canopy cover increases, in other words, there may be an upper limit to forest density for practical use of ITD.

Along with these inherent limitations, past studies using ITD commonly have several characteristics that make application to broad, landscape-level analyses difficult. First, many of the studies are performed in structurally simple forests, where assumptions of even tree spacing, single-layered canopies, or model-conforming crowns are satisfied (Heurich et al. 2004; Bortolot 2006; Barilotti et al. 2009; Stumberg et al. 2014). However, accurate quantification of reference conditions may require operating in more structurally complex forests, where the majority of trees may not be visible to LiDAR sensors and individual trees can have very complex crowns. Second, segmentation algorithms can have different behavior depending on the structural characteristics of the forest under consideration (Kaartinen et al. 2012; Vauhkonen et al. 2012). Effective landscape restoration, however, must deal consistently with a range of structural conditions. Finally, many ITD methods require a manual tuning step, where parameters are chosen by hand to suit the structure of the area of interest (Bortolot & Wynne 2005; Hyyppa et al. 2005; Li et al. 2012). This step is impractical to carry out for the whole range of structural conditions over a large restoration planning area. These difficulties must be considered before applying ITD across heterogeneous landscapes.

My overarching goal is to determine whether and when ITD is an appropriate tool for assessing vertical and horizontal elements of forest structure across landscape restoration project areas. Specifically, I seek to answer these questions:

1. What forest structural characteristics affect the accuracy of ITD when applied across a diverse landscape?

2. Can ITD be effective across the wide range of structural conditions (including complex forests) necessary for silvicultural restoration?

To meet these objectives, I installed nineteen 0.25-ha stem map plots capturing a diversity of forest structure and representing the range of conditions across an actual landscape restoration project and a potential reference area. Using LiDAR data acquired over these locations, I assessed the accuracy of a simple ITD method at my stem map plots, compared my results to those of existing ITD studies, assessed which trees were and were not successfully identified, and investigated the ability of various forest structural characteristics to explain ITD accuracy.

Methods

Study areas

My sample sites for this study are located in two areas on the western slope of the Sierra Nevada of California, USA (Figure 2): Yosemite National Park (Yosemite) and the Dinkey Landscape Restoration Project area in and around the Dinkey Creek watershed of the Sierra National Forest and adjacent private forestlands (Dinkey). I selected these areas with the goal of capturing the elements of an actual restoration project. The areas include a wide range of forest structural conditions that are representative of the mid-montane Sierra Nevada as a whole, and incorporate potential reference areas that have been managed as wilderness as well as an active restoration project area that has a long history of commercial and recreational use.

Yosemite is one of the oldest (est. 1890) and largest (3027 km^2) parks in the United States National Park system. The vast majority of the park has never been subject to commercial timber harvest, and 94% of park land is retained as designated wilderness. Wildfire was suppressed in Yosemite from 1891 until 1972, when the park began to allow wildfires to burn if permitted by safety and air quality standards. In addition to these “wildland use fires,” the park began an active prescribed burning program in 1970 (van Wagtendonk and Lutz 2007). The limited degree

of active management and the rich fire history combine to offer a complex mosaic of forest structural conditions.

Dinkey is a 623 km^2 area managed under the Collaborative Forest Landscape Restoration Program (Dinkey Project Planning Forum 2010). The area saw light use by prospectors mining gold and tungsten in the late 19th century and heavy use by shepherds and cattlemen from the 1860s until 1905, when the formation of the Forest Service led to better enforcement of land use regulations. Development of the area by the Civilian Conservation Corps in the 1930s led to viable commercial logging operations, which peaked in the 1950s and were mostly defunct by the 1980s (Sierra National Forest 1997). Logging practices generally focused on selective harvest of only the most valuable trees; on federal land most trees under 60 cm diameter at breast height (DBH) were retained and many seed and cull trees were left standing (Laudenslayer & Darr 1990). Contemporarily, Dinkey is a popular recreation destination, and federal forest lands are generally interspersed with private timber and residential properties (Dinkey Project Planning Forum 2010). Fire has been excluded from the area since at least the late 19th century, and although the Sierra National Forest began a prescribed burning program in 1994, most of Dinkey has not yet seen the reintroduction of fire (Dinkey Collaborative Group 2010; CALFIRE 2015).

I located my sample sites within sugar pine-white fir (*Pinus lambertiana-Abies concolor*) and red fir (*A. magnifica*) forest types, since these are abundant throughout the Sierra Nevada and because many prospective restoration projects will be occurring in these types (Ansley & Battles 1998; North et al. 2012). Sites range in altitude from 1570 to 2600 m. Climate at the sites is Mediterranean, with less than 3% of precipitation falling during the summer months and most of the precipitation falling as snow. For the period from 1981-2010, annual precipitation ranged from 900 to 1200 mm, minimum January temperature ranged from -6.7 to 1.3 °C, and maximum

July temperature ranged from 19.5 to 26.5 °C (ClimateWNA 2015). Sites in Yosemite had not experienced active forest management, while most sites in Dinkey had been thinned or selection logged. Sites in Yosemite had highly variable fire histories including low, moderate, and high severity fires dating from 1988 to 2013, along with 3 sites that had not burned since at least 1930. Sites in Dinkey had not experienced fire since the onset of fire suppression in the late 19th century.

LiDAR data

Three LiDAR acquisitions were used in this study: Dinkey 2010 and 2012, and Yosemite 2013 (Table 1; Figure 2). Dinkey 2010 and 2012 were collected by Watershed Sciences, Inc. of Corvallis, OR, and Yosemite 2013 was collected by the National Center for Airborne Laser Mapping. Average pulse density ranged from 8.8 to 12.2 pulses m^{-2} across the three acquisitions. The vendors used TerraScan and TerraModeler (Terrasolid Oy, Helsinki, Finland) software to create 1 m resolution digital terrain models (DTMs) from the LiDAR, which were delivered along with the point clouds. DTM values were subtracted from point cloud elevations to create ground-normalized point clouds.

Site selection

Sites were selected with the goal of capturing the range of structural diversity across the sampled forest types. To achieve this, I stratified my sampling using LiDAR-derived structure classes, which has been shown to improve model performance and broaden model applicability compared to simple random sampling or stratification by habitat type (Hawbaker et al. 2009; Maltamo et al. 2010). To create the classes, I used methods similar to Kane et al. (2010b, 2013). The classes are meant to differentiate structure based on ecologically relevant characteristics such as tree height, canopy cover, canopy complexity, and the vertical distribution of foliage.

Structure classes were created for the spatial union of all areas with LiDAR coverage; the most recent data were used for each area. LiDAR metrics were calculated from the ground-normalized point cloud on a 30 m grid using the Fusion LiDAR Toolkit (version 3.4, http://forsys.cfr.washington.edu/fusion.html). Metrics calculated were 25^{th} and 95^{th} percentile heights (corresponding to the approximate base and top of the canopy; Kane et al. 2013), rumple (an index of canopy roughness), total canopy cover >2 m, and stratified canopy cover with break points at 2, 8, 16, and 32 m (providing a coarse canopy profile). The remaining processing was carried out in the R environment (R Development Core Team 2015). The structure classes were derived using a hierarchical classification with Euclidean distances and Ward's linkage method on the LiDAR metrics at a random sample of 15,000 grid cells across the acquisitions. I chose to cut the hierarchical classification tree at 8 classes based on interpretation of the cluster dendrogram and scree plot. Structure classes were then imputed to the whole project area using the Random Forest algorithm (Breiman 2001) in the package yaImpute (Crookston & Finley 2008). The subsampling and imputation was necessary due to high processing demands for hierarchical classification. The resultant structure classes (Figure 3) should represent most of the range of structural diversity present across the LiDAR acquisitions.

Sites were restricted to the chosen forest types (sugar pine-white fir and red fir) using published vegetation maps for Yosemite (Keeler-Wolf et al. 2012) and Dinkey (USDA 2014). Sampling effort per structure class was assigned in proportion with class abundance by forest type. Sites were additionally constrained to be in areas of contiguous structural classification to diminish the edge effects of pixel-based classification: pixels were considered as candidates for plots only if classified the same as all 8 neighbors, that is, plots were only placed within a contiguous patch of at least 0.81 ha in size.

Forty potential plot locations were randomly selected from all areas meeting these criteria. Each location was randomly assigned a priority, and plots were visited in the field accordingly. No plots were located in structure class 1 since that class existed almost exclusively in *Pinus ponderosa* forest types and was outside of the scope of this study.

Field data

Of the 40 identified potential plot locations, 14 were installed in Yosemite in July 2014 and 5 were installed in Dinkey in September 2014. Some plots were rejected upon visitation. Reasons for rejection included that the plots were located in sensitive or high-traffic areas (e.g., the Merced Grove of *Sequoiadendron giganteum*), were on private property, or because the actual vegetation composition did not correspond to the published vegetation maps used in site selection.

Plots were navigated to using a handheld Garmin GPS. When the GPS indicated close proximity to the plot location, a control corner was placed 5 paces away in a random direction. By default, the control corner was the SW corner of the plot. If this default configuration would have been problematic (e.g., a road, cliff, or major rock outcrop would have become a dominant feature within the plot), the plot was rotated clockwise around the control corner in 90° increments until deemed suitable. Each plot was installed as a 0.25 ha square oriented N-S. Plot boundaries were laid out from the control corner using a hand compass and a laser rangefinder.

Control corners were georeferenced using a Trimble GeoXH 2005 Series GPS (Trimble Navigation, Ltd., Sunnyvale, CA). The GPS unit was placed at 2 m height in an area of open canopy near the control corner. The offset of the unit relative to the control corner was recorded using a staff compass and laser rangefinder. GPS points were recorded at 1-second intervals with

5-15 minute residence times. GPS positions were differentially corrected using GPS Pathfinder Office version 5.30 (Trimble Navigation Ltd.). The measured offset was applied to the corrected positions to obtain a final point for the control corner.

All live trees greater than 10 cm diameter at breast height (1.37 m; DBH) and all snags greater than 25 cm DBH were mapped and measured. Mapping was carried out using an electronic compass or angle encoder and a laser rangefinder mounted on a surveying tripod. Plots were surveyed in a single, closed-loop traverse of between 1 and 6 survey stations. Effort was made to minimize the number of long shots (>30 m slope distance) and shots through dense foliage. All plot corners were included in the survey traverse. Locations of trees and the remaining plot corners were then georeferenced with respect to the GPS-derived location of the control corner.

For each tree measured I recorded DBH (to the nearest 0.25 cm) and lean condition (angle from vertical in 5° increments and azimuth of lean to the nearest 1°). For a random subset of 10% of the live trees on each plot, I measured height using a laser hypsometer, and average crown spread by using a clinometer to sight plumb and stretching a steel tape to the bole face at breast height. One half of the measured DBH was added to crown spread measurements to arrive at the crown radius from pith.

I modeled height and crown spread for all trees using linear regression models that I developed from the measured subset (Appendix A). I corrected the mapped coordinates of each tree using the height and lean data so that the coordinates represented the treetop, rather than the breast height location.

LiDAR processing

To delineate individual trees from LiDAR I used the watershed transform (Figure 4). I chose the watershed transform method over the numerous other published ITD methods in part because it is based purely on morphology of the canopy surface. Since it does not require assumptions or prior knowledge about crown widths, tree allometry, forest density, etc., I expect that it is well-suited to consistent performance across a wide range of forest structural conditions. Additionally, the watershed transform is frequently used and freely available (Chen et al. 2006, Edson & Wing 2011, Kaartinen et al. 2012), making it a good standard choice.

I also performed all analyses using a variable window local maxima method, which, like the watershed transform, is commonly used and freely available (Edson & Wing 2011, Vauhkonen et al. 2012, Swetnam & Falk 2014). Methods and results for the local maxima analysis were not appreciably different from the watershed transform method, and so I will hereafter focus only on the watershed transform. The local maxima work is reported in Appendix B.

The watershed transform algorithm operates based on one input: the canopy surface model (CSM), which is created by overlaying a grid on a ground-normalized LiDAR point cloud and assigning each grid cell the value of the highest point within that cell. The characteristics of the segmentation result can be modified to some extent by altering the characteristics of the CSM. In particular, the CSM can be (1) constructed at varying resolutions – finer resolutions retain more detail but have more noise, while coarser resolutions are cleaner but contain less information – and (2) smoothed with different sizes of filter – smaller smoothing windows maintain more fidelity while larger smoothing windows can remove undesirable artifacts. Determining the optimal choice of resolution and smoothing parameters, which should balance retention of detail with removal of noise, comprises the “algorithm tuning” process.

Many ITD studies incorporate a manual or semi-manual tuning step where parameters are optimized based on ground truth plots or visual assessment before being applied to the larger study area. However, this is not practical when analyzing a large area with diverse structure, since the manual tuning would have to be repeated many times to accommodate different conditions.

I carried out a small sub-study investigating the tuning of parameters, documented fully in Appendix B. In short, I determined that selecting CSM resolution and smoothing based on canopy cover provided accuracy comparable to manual tuning using ground truth plots. Since canopy cover can be accurately measured by LiDAR (Korhonen et al. 2011), it is practical to use over large areas. The CSM resolution and smoothing choices used in the remainder of this study were derived from the analysis in Appendix B, and should be applicable to montane Sierra Nevada forests in general.

I created a CSM for each plot, buffering the plot quadrangle by 50 m to eliminate edge effects. Canopy cover was calculated as the proportion of all LiDAR returns within the plot with a height greater than or equal to 2 m. For plots with canopy cover < 30%, CSM resolution was 1 m and no smoothing filter was applied. For plots with canopy cover ≥30% but ≤70%, CSM resolution was 0.5 m and a 3×3 pixel window mean filter was applied. For plots with canopy cover >70%, CSM resolution was 0.25 m and a 5×5 pixel window mean filter was applied (Appendix B).

Finally, I carried out the segmentation using TreeSeg, a prototype tool under development for the Fusion LiDAR Toolkit (http://forsys.cfr.washington.edu/fusion.html). TreeSeg is an implementation of the watershed transform (Vincent & Soille 1991).

Assessing the accuracy of individual tree detection

The key step in credible evaluation of ITD results is associating objects segmented from LiDAR data with actual trees measured in the field. Without this step there is no way of ensuring that counts of segmented objects are in one-to-one correspondence with field counts of trees. I will hereafter refer to objects segmented from the LiDAR as candidate trees, and trees measured in the field will be field trees. I assessed the quality of association between candidate trees and field trees on my plots using methods similar to Vauhkonen et al. (2012). I selected this method because it was the most stringent evaluation method encountered in a review of ITD literature (Appendix C).

The Vauhkonen et al. (2012) method associates candidate trees with field trees by comparing *xyz*-coordinates of candidate tree maxima to those of field treetops. First, the 3-dimensional position of the maximum point of each candidate tree is extracted from the CSM. Any maxima within the 2-dimensional crown spread of a field tree are accepted as candidates for association with that field tree. Then, the best candidate for each field tree is selected by taking the candidate tree maximum with the smallest 3-dimensional distance from that field tree's apex (Figure 5). Lastly, after all possible associations are made, any pairs farther apart than 5 m in 3-dimensional space are taken to be spurious associations, and are considered as no match found.

After matching candidate trees with field trees, I calculated the following evaluation metrics:

1. Error rate of omission, that is, field trees that could not be associated with any candidate tree,
2. Error rate of commission, that is, candidate trees that could not be associated with any field tree, and

3. The *F*-score, a summary statistic that evenly balances omission rates with commission rates (Li et al. 2012).

To calculate the *F*-score, two ratios are first calculated:

$$r = \frac{TP}{TP+FN}, \text{ and} \qquad (1)$$

$$p = \frac{TP}{TP+FP}, \qquad (2)$$

where *TP* is the number of true positives (successful matches), *FN* is the number of false negatives (omitted trees), and *FP* is the number of false positives (committed segments). The *F*-score is then calculated as follows:

$$F = 2 \times \frac{r \times p}{r+p}. \qquad (3)$$

The *F*-score integrates errors of omission and commission into one statistic. Values range from 0 when no trees are successfully matched to 1 when all trees are detected and no erroneous segments are created.

The influence of structure on tree detection

According to my question (1), I wanted to investigate how different forest structural characteristics affect ITD accuracy. I selected a variety of common structural metrics derived from plot and LiDAR data that I suspected may influence ITD results (Table 2). Because of the high degree of multicollinearity among these variables, I performed a principal components analysis (PCA) to reduce the metrics to a smaller set of orthogonal dimensions (McCune & Grace 2002). The PCA was carried out in the R environment (R Core Team 2015) using the vegan package's `rda()` function (Oksanen et al. 2015). I scaled all input metrics to equal variance in order to remove the effect of different measures in different units.

To analyze the relationship between the structural metrics (i.e., the principal component [PC] axes) and ITD accuracy, I used the vegan package's `envfit()` function (Oksanen et al. 2015) to fit the ITD evaluation metrics (omission rate, commission rate, and *F*-score) onto the PCA. Pseudo-significance was evaluated for these fits using a permutation test (McCune & Grace 2002; Oksanen et al. 2015) with 999 permutations of each fitted variable. The goodness of fit statistic, r^2, was calculated as 1 minus the ratio of within-group sum of squares to total sum of squares (Oksanen et al. 2015).

Comparing results to existing studies

According to my question (2), I wanted to determine whether ITD can be used effectively across a wide variety of structural conditions. I met this goal by comparing my ITD accuracy results to results from existing literature, so that effectiveness across a variable landscape can be put into perspective against accuracy evaluated under more ideal circumstances.

I reviewed 73 ITD methods from 34 studies (Appendix C) and selected the 58 which reported at least one of omission, commission, and detection rates. I performed graphic comparisons of my omission, commission, and detection rates versus the same metrics from reviewed studies.

In my review, I identified a major theme in segmentation accuracy: detection rates are much higher for more dominant trees, while understory trees are rarely detected. To determine whether this pattern held across my sample sites, I looked at tree detection rates as a function of relative tree height. I performed this analysis for each structure class separately as well as for all classes pooled together.

Results

Field data

Nineteen plots were installed, 14 in Yosemite and 5 in Dinkey. Plot locations were geographically distributed throughout the LiDAR acquisition areas (Figure 2), ranging from 1500-2600 m in elevation. The physical setting captured by the sample plots was varied (Table 3). Landforms sampled included ridgetops, sideslopes, and flats. Slope grade ranged from completely flat to very steep, greater than 60%.

Stand conditions were also variable. Density ranged from as low as 82 trees per hectare (TPH) in severely burned plots to as high as 1330 TPH in areas without recent fire, while canopy cover ranged from 15-78%. Regardless of density, most plots had a substantial large tree component. Quadratic mean diameter (QMD) ranged from 22-77 cm, 53% of plots had a QMD ≥50 cm, and 16% of plots had a QMD ≥70 cm. Structure varied somewhat by forest type: white fir-mixed conifer plots were generally denser with smaller trees than red fir plots. Median basal area for both forest types was 60 m^2 ha^{-1}, although red fir had much more variability, representing the sites with both lowest (7 m^2 ha^{-1}) and highest (121 m^2 ha^{-1}) stocking (Table 3).

In terms of structure, the plots captured the range of conditions present in the acquisition areas reasonably well given the small number of plots (Figure 6). Since the plots cover a wide range of physical conditions, fire and management histories, and stand conditions, I am comfortable taking it to be an adequate characterization of landscape-level variability.

Assessing the accuracy of individual tree detection

The ITD evaluation metrics varied considerably among plots. Omission rates ranged from 36-78%, while commission rates ranged from 6-343% (Table 4). The *F*-score, which integrates measures of omission and commission, had a mean of 0.45 and standard deviation of 0.13.

A large portion of the commission error was attributed to 3 plots: Y05, Y06, and Y08. These plots had very high rates of commission (343%, 111%, and 191%, respectively) due to oversegmentation. Disregarding these plots, the range of commission rates was 6-71%.

The influence of structure on tree detection

The principal components analysis (PCA) revealed relationships between error rates and plot structural characteristics (Figure 7). The first principal component (PC) explained 54% of the variance in the structural data and was strongly associated with dominant tree height. The second PC explained an additional 30% of the variance and was strongly associated with tree density. The remaining PCs explained negligible amounts of variation and did not show interpretable trends; thus, I did not include them in this analysis.

Error rates of omission increased with density ($r^2 = 0.16$, $p < 0.10$), while commission rates decreased along the same gradient ($r^2 = 0.32$, $p < 0.01$). However, both omission and commission rates increased with dominant tree height ($r^2 = 0.10$, $p = 0.19$ and $r^2 = 0.19$, $p < 0.10$, respectively). Omission errors were most strongly associated with high basal area and canopy cover, while commission errors were most strongly associated with higher QMD and mean tree height.

The *F*-score, representing overall accuracy, did not show a strong response to density ($r^2 = 0.02$, $p = 0.55$), but was strongly related to maximum tree height ($r^2 = 0.48$, $p < 0.01$). The *F*-score increased (i.e., tree detection accuracy increased) with decreasing maximum tree height.

Comparing results to existing studies

Among the 58 reviewed ITD studies, the median omission rate was 45%, while the median commission rate was 15%. Correspondingly, the median omission rate on my plots was 53% and the median commission rate was 43%. With the removal of the 3 oversegmented plots the median commission rate was reduced to 38% (Figure 8).

As found in the review, taller trees at a given site were much more likely to be detected than shorter trees (Figure 9). This result was consistent across all 7 sampled structure classes, as well as when pooled across structure classes. For the pooled data the trend was nearly linear, with a linear regression predicting an individual tree detection likelihood increase of 10.2 percentage points for each 10 percentage point increase in tree height ($r^2 = 0.92$, $p < 0.001$), and with average detection rates ranging from 4.8% for the shortest trees to 98% for the tallest trees.

Discussion

Individual tree detection accuracy in comparison to existing studies

I found that individual tree segmentation on my sample plots did not perform as well as most published tree segmentation results: my median error rate of omission was slightly higher than the median for reviewed studies, while my median commission rate was much higher (Figure 8). This discrepancy can probably be explained by three factors: (1) different segmentation methods, (2) different evaluation methods, and (3) substantive differences in forest structure.

The effect of different segmentation methods on accuracy of results is unclear. Kaartinen et al. (2012) and Vauhkonen et al. (2012) performed studies similar to one another, in which several different ITD algorithms were run on the same datasets and results were compared. While both studies produced a set of front-runners, neither could unequivocally identify the "best" technique. Furthermore, algorithms were generally found to perform better in the forest types for which they were originally developed, indicating that there is probably not any one method that is best for all circumstances.

In this study, I selected the watershed transform algorithm because of its simple, morphological basis, its ubiquity in free software packages, and its ease of implementation. I achieved similar results using the local maxima method (Appendix B), which is also free and easy to use. Because the question of which segmentation methods consistently offer the best results across diverse forest types is still open, I suggest that simplicity and availability are adequate criteria for algorithm selection.

The effect of different evaluation methods is similarly obscure. ITD evaluation methodology is not consistent across the literature: studies vary in (1) how the "truth" data are obtained, (2) whether understory trees are considered in accuracy calculations, and (3) how LiDAR-identified objects are matched to trees from the truth dataset.

For this study, I used the most rigorous evaluation criteria I found in the literature, which was not done by the majority of published work. To evaluate ITD at my sites, I used (1) an accurately field mapped and georeferenced ground truth dataset, (2) included all mapped trees 10 cm DBH or larger in my accuracy calculations, and (3) used a rigorous method of associating LiDAR objects with mapped trees (Vauhkonen et al. 2012), in which ground and LiDAR treetops are

required to have close proximity in 3-dimensional space. I was unable to find any literature quantifying how different choices might have affected apparent ITD accuracy. However, experience suggests that using more lenient methods – for example, (1) generating a truth dataset by manual extraction of trees from orthophotos or from the LiDAR point cloud (e.g., Koukoulas & Blackburn 2005, Rahman & Gorte 2009), (2) ignoring subdominant/understory trees in accuracy calculations (e.g., Schardt et al. 2002), or (3) using a less rigorous association method (e.g., Persson et al. 2002, Leckie et al. 2003) – could result in inflated measures of accuracy.

Clearly, making direct comparisons across different studies can be tenuous. Nevertheless, I have the goal of determining whether ITD is an appropriate tool across heterogeneous landscapes, and to do this does require making direct comparisons to other studies. Recognizing this difficulty, I have chosen what I view as a conservative approach: employ the most rigorous standards in evaluating my own work and compare my work to other studies as if they all had performed equally rigorous evaluations. In this way, I can be sure that the comparison at least provides an upper bound on the discrepancy between my study and others.

Structure of evaluated forests is likely the most significant variable determining success of tree segmentation, since forest structure determines what is and is not sensed by LiDAR, i.e., the raw material of ITD. More complex canopy structure (e.g., large trees, high stocking, and a high degree of variability in the vertical distribution of canopy) contributes to an increase in error rates (Figure 7). This is probably the primary reason for my high error rates compared to past work: while my sample plots were generally located in forests with some component of old trees and, accordingly, variability in the vertical distribution of canopy, the majority of studies I compared to took place in simple, young plantation forests. I discuss the relationship between forest structure and ITD error in more detail in the following section.

The influence of structure on tree detection

At the tree level, the likelihood of being detected was directly related to relative height, that is, a tree's height compared to other trees on the site (Figure 9). Assuming that almost all immediately dominant trees are successfully detected, this is equivalent to the assertion that as a tree becomes shorter relative to its neighbors its chances of being immediately dominant are reduced. This result is corroborated quantitatively by Jakubowski et al. (2013), who found that tree detection rates decreased nearly linearly with lower canopy positions, and is reported qualitatively in nearly every tree segmentation study. Furthermore, the trend was consistent across all 7 of the sampled structure classes, indicating that it holds equally across a wide range of conditions, irrespective of other elements of structure.

At the plot level, my three ITD evaluation metrics – omission error rates, commission error rates, and the *F*-score – all exhibited different responses to changes in forest structure. I defined structure by two principal dimensions: dominant tree height and density (Figure 7). Within the space defined by these principal component axes, I also looked at trends in several other structural attributes (Table 2).

Error rates of omission increased with dominant tree height. This is in line with my finding that shorter trees on a site are less likely to be detected. When the dominant tree height increases, the dominant canopy stratum is occupied by fewer, larger trees (Franklin et al. 2002). This means that a greater proportion of trees are in non-dominant canopy strata, and are obscured from LiDAR.

Omission rates also increased with increasing density. This is not surprising: the same result was reported by Vauhkonen et al. (2012), and Swetnam & Falk (2014) and Tao et al. (2014) proposed

crown overlap – which is related to density – as a factor influencing omission rates. Increased density necessarily means a decrease in space between trees, and therefore a loss of crown differentiation.

Of the structural attributes tested, omission error was most closely related to basal area and canopy cover. These metrics are both especially responsive to the presence of large trees on a site, indicating once again that the physical barrier created by large canopies is likely the primary impediment to tree detection.

Error rates of commission, like omission rates, increased with dominant tree height; however, commission rates decreased with increasing density. Commission error was most closely associated with increasing quadratic mean diameter and mean tree height, both measures of the average tree size. Taken together, these relationships present a consistent story: error rates of commission seem to increase with increasing complexity of individual tree crowns. As trees become larger (and older), their crowns deviate from model conformance and begin to develop complexity and individuality (Ishii et al. 2004; Van Pelt & Sillett 2008). Since ITD algorithms essentially require model-conforming crown morphology, they do not behave well for trees with complex crowns. In particular, large orthotropic limbs can be mistaken for treetops and crown reiterations can be erroneously counted as additional trees, since both present local maxima that are difficult to distinguish from individual trees.

The negative relationship between commission rates and density is consistent with this narrative. Lower density sites have more growing space per tree, so each individual tree is able to support more crown volume. Trees under more open conditions are under less pressure to grow vertically, and allocate more resources to horizontal crown spread. Conversely, higher density

sites have less growing space per tree, which induces crown simplifying responses such as self-pruning and model-conforming vertical growth (Jack & Long 1991; Purves et al. 2007).

The *F*-score, which integrates omission and commission rates, increased (improved) with decreasing dominant tree height, but did not respond to density, due apparently to the cancelling of the opposing effects of density on omission and commission error rates. Overall improvement of the *F*-score with decreasing dominant height may be driven in part by the direct relationship between dominant height and vertical variability in the canopy: shorter canopies are correlated with less vertical complexity, which should improve ITD results. However, the relationship between the *F*-score and maximum height ($r^2 = 0.64$, $p < 0.001$) is stronger than the relationship between the *F*-score and variance ($r^2 = 0.54$, $p < 0.001$), standard deviation ($r^2 = 0.58$, $p < 0.001$), or coefficient of variation of height ($r^2 = 0.14$, $p = 0.12$), indicating that there is probably something about height *per se* that drives ITD success more directly than variability in height does. One possibility is that dominant height acts as a proxy for age, and forest aging generally results in increased complexity at multiple scales (Kane et al. 2011).

In summary, the reliability of ITD at a given site is best predicted by the height of the tallest trees, because taller trees have larger crowns and obscure the lower canopy strata. In denser stands, most of the errors in ITD are errors of omission, since individual crowns become less differentiated as stocking increases. In less dense stands, most of the errors are errors of commission, because trees that have more growing space have larger and more complex crowns that are more likely to present multiple local maxima points for a single tree. But density is not a good predictor of ITD accuracy, since its opposing effects on omission and commission error rates approximately cancel out.

Strengths and limitations of individual tree detection

My overarching goal was to determine whether and when ITD is an appropriate tool for assessing forest structure across landscape restoration project areas. I have found that, while performing ITD over heterogeneous landscapes is less accurate than more homogeneous landscapes, the fundamental structural units that are being detected are the same: dominant trees. No other class of trees could be reliably segmented. This means that ITD can be used effectively to estimate parameters and processes driven by the largest, most dominant trees, but is probably very poor at predicting attributes driven by the smaller trees.

Luckily, the largest trees do dominate several important aspects of ecosystem function. For one, a small percentage of the large trees make up the vast majority of the biomass for many forest stands (Lutz et al. 2012; Bastin et al. 2015). This has many ramifications, since biomass is directly related to aboveground carbon storage, merchantable wood volume, and stocking levels, and can sometimes be used to predict compositional diversity in terms of species richness (Chisholm et al. 2013). The largest trees are also the sites of the most rapid carbon accumulation, since larger trees have higher relative growth rates than smaller trees (Sillett et al. 2010, Stephenson et al. 2014); this can be used to estimate potential strength of a stand as a carbon sink. Furthermore, large trees tend to dominate the spatial heterogeneity within a stand, acting as key drivers in the horizontal arrangement of structure (Lutz et al. 2013); the particular *xy*-locations of dominant trees detected from LiDAR could potentially be used to infer some elements of spatial pattern. Lastly, large trees provide unique structures that are keystone elements of many vertebrate species' habitat requirements (Tews et al. 2004).

On the other hand, several aspects of structure and function are driven by small trees. For example, the smaller trees dominate stand density (Lutz et al. 2012) and crown fire risk (i.e.,

ladder fuels; Agee & Skinner 2005), and contribute greatly to hiding cover for wildlife species (Millspaugh et al. 1998; Zielinski et al. 2004). Sometimes, such as in the case of fire risk, this is not an issue: continuity between the ground and upper canopy can be quantified from the LiDAR point cloud without any idea of what points are associated to particular trees (Erdody & Moskal 2010). However, at other times the lack of distinction between small trees becomes problematic. For instance, ITD is probably unable to distinguish a single dominant shade-tolerant tree with a deep canopy from a top-loaded shade-intolerant with a smaller tree growing up underneath it, which could be a shortcoming when planning silvicultural restoration.

Conclusions

LiDAR individual tree detection across a structurally diverse landscape restoration project area is less accurate than across the smaller and less diverse areas over which it has previously been studied. However, the trees that are detected are similar in both cases: regardless of forest structure, canopy dominants are very likely to be detected and relatively shorter trees are very unlikely to be detected.

ITD is not very effective as a direct replacement for traditional inventory in structurally complex forests, since shorter trees – which are the majority by numbers – are likely to be missed. Correspondingly, metrics dominated by shorter trees, such as stand density, are not likely to be predicted well. However, canopy dominants can be detected reliably, and metrics that are driven by large trees, such as biomass, basal area, and spatial heterogeneity, can probably be predicted well.

In the context of landscape restoration in the Sierra Nevada, ITD can be an appropriate tool for describing reference areas and treatment units, since it behaves consistently across the breadth of

structural conditions present. However, the strengths and limitations identified in this study must be duly considered. When used correctly, ITD has the potential to accurately describe characteristics of dominant tree structure at a fine scale over large and diverse landscapes.

References

Agee, J.K. & C.N. Skinner. 2005. Basic Principles of Forest Fuel Reduction Treatments. *Forest Ecology and Management* **211**: 83-86.

Ansley, J.-A.S. & J.J. Battles. 1998. Forest Composition, Structure, and Change in Old-Growth Mixed Conifer Forest in the Northern Sierra Nevada. *Journal of the Torrey Botanical Society* **125(4)**: 297-308.

Barilotti, A., F. Crosilla, and F. Sepic. 2009. Curvature analysis of LiDAR data for single tree species classification in alpine latitude forests. *IAPRS Laser scanning* **38(3)**: 129-134.

Bastin, J.-F., N. Barbier, M. Réjou-Méchain, A. Fayolle, S. Gourlet-Fleury, D. Maniatis, T. de Haulleville, F. Baya, H. Beeckman, D. Beina, P. Couteron, G. Chuyong, G. Dauby, J.-L. Doucet, V. Droissart, M. Dufrêne, C. Ewango, J.F. Gillet, C.H. Gonmadje, T. Hart, T. Kavali, D. Kenfack, M. Libalah, Y. Malhi, J.-R. Makana, R. Pélissier, P. Ploton, A. Serckx, B. Sonké, T. Stevart, D.W. Thomas, C. De Cannière, and J. Bogaert. 2015. Seeing Central African forests through their largest trees. *Nature Scientific Reports* **5**: Online only.

Bewley, R.H., S.P. Crutchley, and C.A. Shell. 2005. New light on an ancient landscape: lidar survey in the Stonehenge World Heritage Site. *Antiquity* **79**: 636-647.

Bortolot, Z.J. 2006. Using Tree Clusters to Derive Forest Properties from Small Footprint Lidar Data. *Photogrammetric Engineering & Remote Sensing* **72(12)**: 1389-1397.

Bortolot, Z.J. & R.H. Wynne. 2005. Estimating forest biomass using small footprint LiDAR data: An individual tree-based approach that incorporates training data. *ISPRS Journal of Photogrammetry & Remote Sensing* **59**: 342-360.

Breidenbach, J., E. Næsset, V. Lien, T. Gobakken, and S. Solberg. 2010. Prediction of species specific forest inventory attributes using a nonparametric semi-individual tree crown approach based on fused airborne laser scanning and multispectral data. *Remote Sensing of Environment* **114**: 911-924.

Breiman, L. 2001. Random Forests. *Machine Learning* **45**: 5-32.

California Department of Forestry and Fire Protection 2015. Fire Perimeters 2014 version 2 (firep14_2). (accessed July 23, 2015). Vector digital data.

Chen, Q., D. Baldocchi, P. Gong, and M. Kelly. 2006. Isolating Individual Trees in a Savanna Woodland Using Small Footprint Lidar Data. *Photogrammetric Engineering & Remote Sensing* **72(8)**: 923-932.

Chisholm, R.A., H.C. Muller-Landau, K.A. Rahman, D.P. Bebber, Y. Bin, S.A. Bohlman, N.A. Bourg, J. Brinks, S. Bunyavejchewin, N. Butt, H. Cao, M. Cao, D. Cárdenas, L. Chang, J. Chiang, G. Chuyong, R. Condit, H.S. Dattaraja, S. Davies, A. Duque, C. Fletcher, N. Gunatilleke, S. Gunatilleke, Z. Hao, R. Harrison, R. Howe, C. Hsieh, S.P. Hubbell, A. Itoh, D. Kenfack, S. Kiratiprayoon, A.J. Larson, J. Lian, D. Lin, H. Liu, J.A. Lutz, K. Ma,

Y. Malhi, S. McMahon, W. McShea, M. Meegaskumbura, S. M. Razman, M.D. Morecroft, C.J. Nytch, A. Oliveira, G.G. Parker, S. Pulla, R. Punchi-Manage, H. Romero-Saltos, W. Sang, J. Schurman, S. Su, R. Sukkumar, I. Sun, H.S. Suresh, S. Tan, D. Thomas, S. Thomas, J. Thompson, R. Valencia, A. Wolf, S. Yap, W. Ye, Z. Yuan, and J. Zimmerman. 2013, Scale-dependent relationships between tree species richness and ecosystem function in forests. *Journal of Ecology* **101**: 1214-1224.

Churchill, D.J., A.J. Larson, M.C. Dahlgreen, J.F. Franklin, P.F. Hessburg, and J.A. Lutz. 2013. Restoring forest resilience: From reference spatial patterns to silvicultural prescriptions and monitoring. *Forest Ecology and Management* **291**: 442-457.

ClimateWNA 2015. ClimateWNA: A Program to generate climate normal data for genecology and climate change stuides in western North America (WWW Document). < http://www.genetics.forestry.ubc.ca/cfcg/ClimateWNA/ClimateWNA.html> (accessed July 20, 2015).

Covington, W.W. & M.M. Moore. 1994. Southwestern Ponderosa Forest Structure: Changes since Euro-American settlement. *Journal of Forestry* **92(1)**: 39-47.

Crookston, N.L. & A.O. Finley. 2008. yaImpute: An R Package for kNN Imputation. *Journal of Statistical Software* **23(10)**: Online only.

Dinkey Collaborative Group 2010. Dinkey Collaborative Landscape Restoration Strategy. USDA Forest Service Pacific Southwest Region.

Dinkey Project Planning Forum 2010. Collaborative Forest Landscape Restoration Program Proposal: Dinkey Landscape Restoration Project. USDA Forest Service Pacific Southwest Region.

Edson, C. & M.G. Wing. 2011. Airborne Light Detection and Ranging (LiDAR) for Individual Tree Stem Location, Height, and Biomass Measurements. *Remote Sensing* **3**: 2494-2528.

Erdody, T.L. & L.M. Moskal. 2010. Fusion of LiDAR and imagery for estimating forest canopy fuels. *Remote Sensing of Environment* **114**: 725-737.

Falkowski, M.J., A.M.S. Smith, P. Gessler, A.T. Hudak, and L.A. Vierling. 2008. The influence of conifer forest canopy cover on the accuracy of two individual tree measurement algorithms using lidar data. *Canadian Journal of Remote Sensing* **34S2**: S1-S13.

Franklin, J.F., T.A. Spies, R. Van Pelt, A.B. Carey, D.A. Thornburgh, D.R. Berg, D.B. Lindenmayer, M.E. Harmon, W.S. Keeton, D.C. Shaw, K. Bible, and J. Chen. 2002. Disturbances and structural development of natural forest ecosystems with silvicultural implications, using Douglas-fir forests as an example. *Forest Ecology and Management* **155**: 399-423.

Franklin, J.F., R.J. Mitchell, and B.J. Palik. 2007. Natural Disturbance and Stand Development Principles for Ecological Forestry. USDA Forest Service Northern Research Station. General Technical Report NRS-19.

Franklin, J.F., K.N. Johnson, D.J. Churchill, R.K. Hagmann, D. Johnson, and J. Johnston. 2013. Restoration of Dry Forests in Eastern Oregon. The Nature Conservancy, Portland, OR. 202 pp.

French, J.R. 2003. Airborne LiDAR in support of geomorphological and hydraulic modeling. *Earth Surface Processes and Landforms* **28**: 321-335.

Fry, D.L., S.L. Stephens, B.M. Collins, M.P. North, E. Franco-Vizcaíno, and S.J. Gill. 2014. Contrasting Spatial Patterns in Active-Fire and Fire-Suppressed Mediterranean Climate Old-Growth Mixed Conifer Forests. *PLoS One* **9(2)**: Online only.

Hawbaker, T.J., N.S. Keuler, A.A. Lesak, T. Gobakken, K. Contrucci, and V.C. Radeloff. 2009. Improved estimates of forest vegetation structure and biomass with a LiDAR-optimized sampling design. *Journal of Geophysical Research* **114**: Online only.

Hessburg, P.F., J.K. Agee, and J.F. Franklin. 2005. Dry forests and wildland fires of the inland Northwest USA: Contrasting the landscape ecology of the pre-settlement and modern eras. *Forest Ecology and Management* **211**: 117-139.

Hessburg, P.F., D.J. Churchill, A.J. Larson, R.D. Haugo, C. Miller, T.A. Spies, M.P. North, N.A. Povak, R.T. Belote, P.H. Singleton, W.L. Gaines, R.E. Keane, G.H. Aplet, S.L. Stephens, P. Morgan, P.A. Bisson, B.E. Rieman, R.B. Salter, and G.H. Reeves. 2015. Restoring fire-prone Inland Pacific landscapes: seven core principles. *Landscape Ecology* **30(10)**: 1805-1835.

Heurich, M., Å. Persson, J. Holmgren, and E. Kennel. 2004. Detecting and measuring individual trees with laser scanning in mixed mountain forest of Central Europe using an algorithm developed for Swedish boreal forest conditions. *International Archives of Photogrammetry, Remote Sensing, and Spatial Information Sciences* **36**: 307-312.

Huang, H., P. Gong, X. Cheng, N. Clinton, and Z. Li. 2009. Improving Measurement of Forest Structural Parameters by Co-Registering of High Resolution Aerial Imagery and Low Density LiDAR Data. *Sensors* **9**: 1541-1558.

Hummel, S., A.T. Hudak, E.H. Uebler, M.J. Falkowski, and K.A. Megown. 2011. A Comparison of Accuracy and Cost of LiDAR versus Stand Exam Data for Landscape Management on the Malheur National Forest. *Journal of Forestry* **109(5)**: 267-273.

Hyyppä, J., T. Mielonen, H. Hyyppä, M. Maltamo, X. Yu, E. Honkavaara, and H. Kaartinen. 2005. Using individual tree crown approach for forest volume extraction with aerial images and laser point clouds. *ISPRS Laser scanning*: 144-149.

Ishii, H.T., R. Van Pelt, G.G. Parker, and N.M. Nadkarni. 2004. Age-Related Development of Canopy Structure and Its Ecological Functions. IN: Forest Canopies. M.D. Lowman & H.B. Rinker, Ed. Elsevier. 517 pp.

Jaboyedoff, M., T. Oppikofer, A. Abellán, M.-H. Derron, A. Loye, R. Metzger, and A. Pedrazzini. 2012. Use of LIDAR in landslide investigations: a review. *Natural Hazards* **61**: 5-28.

Jack, S.B. & J.N. Long. 1991. Analysis of stand density effects on canopy structure: a conceptual approach. *Trees* **5**: 44-49.

Jakubowski, M.K., W. Li, Q. Guo, and M. Kelly. 2013. Delineating Individual Trees from Lidar Data: A Comparison of Vector- and Raster-based Segmentation Approaches. *Remote Sensing* **5**: 4163-4186.

Kaartinen, H., J. Hyyppä, X. Yu, M. Vastaranta, H. Hyyppä, A. Kukko, M. Holopainen, C. Heipke, M. Hirschmugl, F. Morsdorf, E. Næsset, J. Pitkänen, S. Popescu, S. Solberg, B.M. Wolf, and J.-C. Wu. 2012. An International Comparison of Individual Tree Detection and Extraction Using Airborne Laser Scanning. *Remote Sensing* **4**: 950-974.

Kane, V.R., J.D. Bakker, R.J. McGaughey, J.A. Lutz, R.F. Gersonde, and J.F. Franklin. 2010. Examining conifer canopy structural complexity across forest ages and elevations with LiDAR data. *Canadian Journal of Forest Research* **40**: 774-787.

Kane, V.R., R.F. Gersonde, J.A. Lutz, R.J. McGaughey, J.D. Bakker, and J.F. Franklin. 2011. Patch dynamics and the development of structural and spatial heterogeneity in Pacific Northwest forests. *Canadian Journal of Forest Research* **41**: 2276-2291.

Kane, V.R., M.P. North, J.A. Lutz, D.J. Churchill, S.L. Roberts, D.F. Smith, R.J. McGaughey, J.T. Kane, and M.L. Brooks. 2013. Assessing fire effects on forest spatial structure using a fusion of Landsat and airborne LiDAR data in Yosemite National Park. *Remote Sensing of Environment* **151**: 89-101.

Keeler-Wolf, T., P.E. Moore, E.T. Reyes, J.M. Menke, D.N. Johnson, and D.L. Karavidas. 2012. Yosemite National Park Vegetation and Mapping Project. USDI Park Service Yosemite National Park. Natural Resource Technical Report NPS/YOSE/NRTR-2012/598.

Korhonen, L., I. Korpela, J. Heiskanen, and M. Maltamo. 2011. Airborne discrete-return LIDAR data in the estimation of vertical canopy cover, angular canopy closure and leaf area index. *Remote Sensing of Environment* **115**: 1065-1080.

Kotliar, N.B. & J.A. Wiens. 1990. Multiple Scales of Patchiness and Patch Structure: A Hierarchical Framework for the Study of Heterogeneity. *Oikos* **59(2)**: 253-260.

Koukoulas, S. & G.A. Blackburn. 2005. Mapping individual tree location, height and species in broadleaved deciduous forest using airborne LIDAR and multi-spectral remotely sensed data. *International Journal of Remote Sensing* **26(3)**: 431-455.

Laes, D., S. Reutebuch, R.J. McGaughey, P. Maus, T. Mellin, C. Wilcox, J. Anhold, M. Finco, and K. Brewer. 2008. Practical Lidar-Acquisition Considerations for Forestry Applications. USDA Forest Service Remote Sensing Applications Center, Salt Lake City, UT. RSAC-0111-BRIEF1.

Larson, A.J. & D.J. Churchill. 2012. Tree spatial patterns in fire-frequent forests of western North America, including mechanisms of pattern formation and implications for designing fuel reduction and restoration treatments. *Forest Ecology and Management* **267**: 74-92.

Laudenslayer, W.F., Jr. & H.H. Darr. 1990. Historical Effects of Logging on the Forests of the Cascade and Sierra Nevada Ranges of California. *Transactions of the Western Section of the Wilderness Society* **26**: 12-23.

Leckie, D., F. Gougeon, D. Hill, R. Quinn, L. Armstrong, and R. Shreenan. 2003. Combined high-density lidar and multispectral imagery for individual tree crown analysis. *Canadian Journal of Remote Sensing* **29(5)**: 633-649.

Li, W., Q. Guo, M.K. Jakubowski, and M. Kelly. 2012. A New Method for Segmenting Individual Trees from the Lidar Point Cloud. *Photogrammetric Engineering & Remote Sensing* **78(1)**: 75-84.

Lutz, J.A., A.J. Larson, M.E. Swanson, and J.A. Freund. 2012. Ecological Importance of Large-Diameter Trees in a Temperate Mixed-Conifer Forest. *PLoS One* **7(5)**: Online only.

Lutz, J.A., A.J. Larson, J.A. Freund, M.E. Swanson, and K.J. Bible. 2013. The Importance of Large-Diameter Trees to Forest Structural Heterogeneity. *PLoS One* **8(12)**: Online only.

Lydersen, J.M., M.P. North, E.E. Knapp, and B.M. Collins. 2013. Quantifying spatial patterns of tree groups and gaps in mixed-conifer forests: Reference conditions and long-term changes following fire suppression and logging. *Forest Ecology and Management* **304**: 370-382.

Maltamo, M., O.M. Bollandsås, E. Næsset, T. Gobakken, and P. Packalén. 2010. Different plot selection strategies for field training data in ALS-assisted forest inventory. *Forestry* **84(1)**: 23-31.

McCune, B., J.B. Grace, and D.L. Urban. 2002. Analysis of Ecological Communities. MjM Software Design, Gleneden Beach, OR. 300 pp.

Millspaugh, J.J., K.J. Raedeke, G.C. Brundige, and C.C. Willmott. 1998. Summer Bed Sites of Elk (*Cervus elaphus*) in the Black Hills, South Dakota: Considerations for Thermal Cover Management. *American Midland Naturalist* **139**: 133-140.

Moore, M.M., W.W. Covington, and P.Z. Fulé. 1999. Reference conditions and ecological restoration: a Southwestern ponderosa pine perspective. *Ecological Applications* **9(4)**: 1266-1277.

Morsdorf, F., E. Meier, B. Kötz, K.I. Itten, M. Dobbertin, and B. Allgöwer. 2004. LIDAR-based geometric reconstruction of boreal type forest stands at single tree level for forest and wildland fire management. *Remote Sensing of Environment* **92**: 353-362.

North, M.P., P. Stine, K. O'Hara, W. Zielinski, and S. Stephens. 2009. An Ecosystem Management Strategy for Sierran Mixed-Conifer Forests. USDA Forest Service Pacific Southwest Research Station. General Technical Report PSW-GTR0-220 (Second printing with addendum).

North, M.P., B.M. Collins, and S.S. Stephens. 2012. Using Fire to Increase the Scale, Benefits, and Future Maintenance of Fuels Treatments. *Journal of Forestry* **110(7)**: 392-401.

Oksanen, J., F. Guillaume Blanchet, R. Kindt, P. Legendre, P.R. Minchin, R.B. O'Hara, G.L. Simpson, P. Sólymos, M.H.H. Stevens, and H. Wagner.

Packalen, P., J. Vauhkonen, E. Kallio, J. Peuhkurinen, J. Pitkänen, I. Pippuri, J. Strunk, and M. Maltamo. 2013. Predicting the spatial pattern of trees by airborne laser scanning. *International Journal of Remote Sensing* **34(14)**: 5154-5165.

Peterson, D.L., M.C. Johnson, J.K. Agee, T.B. Jain, D. McKenzie, and E.D. Reinhardt. 2005. Forest Structure and Fire Hazard in Dry Forests of the Western United States. USDA Forest Service Pacific Northwest Research Station. General Technical Report PNW-GTR-628.

Purves, D.W., J.W. Lichstein, S.W. Pacala. 2007. Crown Plasticity and Competition for Canopy Space: A New Spatially Implicit Model Parameterized for 250 North American Tree Species. *PLoS One* **2(9)**: Online only.

R Core Team 2015. R: A language and environment for statistical computing. R Foundation for Statistical Computing, Vienna, Austria. URL: http://www.R-project.org.

Rahman, M.Z.A. & B.G.H. Gorte. 2009. Tree crown delineation from high resolution airborne LiDAR based on densities of high points. *ISPRS Laser scanning* **38**: 123-128.

Richardson, J.J. & L.M. Moskal. 2011. Strengths and limitations of assessing forest density and spatial configuration with aerial LiDAR. *Remote Sensing of Environment* **115**: 2640-2651.

Schultz, C.A., T. Jedd, and R.D. Beam. 2012. The Collaborative Forest Landscape Restoration Program: A History and Overview of the First Projects. *Journal of Forestry* **110(7)**: 381-391.

Sierra National Forest 1997. Dinkey Creek: A bridge from past to present [Pamphlet]. USDA Forest Service: Clovis, CA.

Sillett, S.C., R. Van Pelt, G.W. Koch, A.R. Ambrose, A.L. Carroll, M.E. Antoine, and B.M. Mifsud. 2010. Increasing wood production through old age in tall trees. *Forest Ecology and Management* **259**: 976-994.

Stephenson, N.L., A.J. Das, R. Condit, S.E. Russo, P.J. Baker, N.G. Beckman, D.A. Coomes, E.R. Lines, W.K. Morris, N. Rüger, E. Álvarez, C. Blundo, S. Bunyavejchewin, G. Chuyong, S.J. Davies, Á. Duque, C.N. Ewango, O. Flores, J.F. Franklin, H.R. Grau, Z. Hao, M.E. Harmon, S.P. Hubbell, D. Kenfack, Y. Lin, J.-R. Makana, A. Malizia, L.R. Malizia, R.J. Pabst, N. Pongpattananurak, S.-H. Su, I.-F. Sun, S. Tan, D. Thomas, P.J. van Mantgem, X. Wang, S.K. Wiser, and M.A. Zavala. 2014. Rate of tree carbon accumulation increases continuously with tree size. *Nature* **507**: 90-96.

Stumberg, N., O.M. Bollandsås, T. Gobakken, and E. Næsset. 2014. Automatic Detection of Small Single Trees in the Forest-Tundra Ecotone Using Airborne Laser Scanning. *Remote Sensing* **6**: 10152-10170.

Swetnam, T.L. & D.A. Falk. 2014. Application of Metabolic Scaling Theory to reduce error in local maxima tree segmentation from aerial LiDAR. *Forest Ecology and Management* **323**: 158-167.

Tao, S., Q. Guo, L. Li, B. Xue, M. Kelly, W. Li, G. Xu, and Y. Su. 2014. Airborne Lidar-derived volume metrics for aboveground biomass estimation: A comparative assessment for conifer stands. *Agricultural and Forest Meteorology* **199**: 24-32.

Tews, J., U. Brose, V. Grimm, K. Tielbörger, M.C. Wichmann, M. Schwager, and F. Jeltsch. 2004. Animal species diversity driven by habitat heterogeneity/diversity: the importance of keystone structures. *Journal of Biogeography* **31**: 79-92.

Tuten, M.C., A. Sánchez Meador, and P.Z. Fulé. 2015. Ecological restoration and fine-scale forest structure regulation in southwestern ponderosa pine forests. *Forest Ecology and Management* **348**: 57-67.

Underhill, J.L., Y. Dickinson, A. Rudney, and J. Thinnes. 2014. Silviculture of the Colorado Front Range Landscape Restoration Initiative. *Journal of Forestry* **112(5)**: 484-493.

USDA 2013. Red Knight Restoration Project: Environmental Assessment. USDA Forest Service Pacific Northwest Region.

USDA 2014. ExistingVegSouthSierra2000_2008_v1. USDA Forest Service Pacific Southwest Region Remote Sensing Lab, McClellan, CA. Vector digital data.

Van Pelt, R. & S.C. Sillett. 2008. Crown Development of Coastal *Pseudotsuga menziesii*, including a Conceptual Model for Tall Conifers. *Ecological Monographs* **78(2)**: 283-311.

van Wagtendonk, J.W. & J.A. Lutz. 2007. Fire Regime Attributes of Wildland Fires in Yosemite National Park, USA. *Fire Ecology* **3(2)**: 34-52.

Vauhkonen, J., L. Ene, S. Gupta, J. Heinzel, J. Holmgren, J. Pitkänen, S. Solberg, Y. Wang, H. Weinacker, K.M. Hauglin, V. Lien, P. Packalén, T. Gobakken, B. Koch, E. Næsset, T. Tokola, and M. Maltamo. 2012. Comparative testing of single-tree detection algorithms under different types of forest. *Forestry* **85(1)**: 27-40.

Vincent, L. & P. Soille. 1991. Watersheds in Digital Spaces: An Efficient Algorithm Based on Immersion Simulations. *IEEE Transactions on Pattern Analysis and Machine Intelligence* **13(6)**: 583-598.

Wu, J. 1999. Hierarchy and scaling: extrapolating information along a scaling ladder. *Canadian Journal of Remote Sensing* **25(4)**: 367-380.

Yu, X., J. Hyyppä, M. Vastaranta, M. Holopainen, and R. Viitala. 2011. Predicting individual tree attributes from airborne laser point clouds based on the random forests technique. *ISPRS Journal of Photogrammetry & Remote Sensing* **66**: 28-37.

Zielinski, W.J., R.L. Truex, G.A. Schmidt, F.V. Schlexer, K.N. Schmidt, and R.H. Barrett. 2004. Resting habitat selection by fishers in California. *Journal of Wildlife Management* **68(3)**: 475-492.

Table 1 Attributes of LiDAR acquisitions used in this study. Contractor abbreviations: WSI = Watershed Sciences, Inc. of Corvallis, OR; NCALM = National Center for Airborne Laser Mapping.

Acquisition	Dates Acquired	Contractor	Instrument	Max. returns per pulse	Average pulse density (pulses m^{-2})	Laser pulse frequency (kHz)	Field of view (°)	Survey altitude (m agl)	Accuracy (RMSE, cm)
Dinkey 2010	October 12-19 2010	WSI	Dual Leica ALS50 Phase II	4	12.0	>83	28	1100 & 1500	≤15
Dinkey 2012	November 21-27 2012	WSI	Leica ALS60	4	8.8	>96	28	900	≤15
Yosemite 2013	November 6-24 2013	NCALM	Optech ALTM Gemini	4	12.2	125	28	600	≤11

Table 2 Stand structural metrics tested to explain variation in individual tree segmentation accuracy. TPH, BAH, QMD, MeanHt, and MaxHt are derived from ground-based measurements. The remaining metrics are derived from LiDAR.

Abbreviation	Description
TPH	Tree density (number ha^{-1})
BAH	Basal area (m^2ha^{-1})
QMD	Quadratic mean diameter (cm)
CC	LiDAR-measured canopy cover (%)
MeanHt	Mean tree height (m)
MaxHt	Maximum tree height (m)
SD	Standard deviation of all LiDAR return heights
Var	Variance of LiDAR return heights
CV	Coefficient of variation of LiDAR return heights
Skew	Skewness of LiDAR return heights
Kurt	Kurtosis of LiDAR return heights
P25	25^{th} percentile of LiDAR return heights (m)
P95	95^{th} percentile of LiDAR return heights (m)

Table 3 Environmental, physical, and biological conditions at sample plots. For structure class characteristics, see Figure 3. Forest type codes: ABCO = *Abies concolor*-mixed conifer, ABMA = *Abies magnifica*. Slope classes: Flat slopes are <5%, Moderate slopes are 5-25%, and Steep slopes are >25% grade. Fire severity and fire year refer to the most recent fire on record. Fire severity classes: None = no fire since federal forest management, Low = fire with 0-30% overstory mortality, Moderate = fire with 30-70% overstory mortality, High = fire with >70% overstory mortality. CC = canopy cover, TPH = trees per hectare, BAH = basal area per hectare, and QMD = quadratic mean diameter.

Plot	Structure Class	Elevation (m)	Forest type	Slope	Fire severity	Fire year	CC (%)	TPH	BAH ($m^2 ha^{-1}$)	QMD (cm)	Mean height (m)	Max. height (m)
Y07	2	1990	ABMA	Flat	Low	1988	15	173	7	23	10	24
D04	3	1940	ABCO	Flat	None	-	45	641	38	27	13	33
Y11	4	2090	ABMA	Flat	Mod.	2013	36	113	29	57	21	44
Y13	4	2330	ABMA	Mod.	None	-	27	85	18	52	20	37
D01	4	2130	ABCO	Mod.	None	-	38	191	32	46	18	32
Y01	5	1900	ABCO	Flat	Low	2010	75	843	90	36	14	41
Y02	5	1840	ABCO	Steep	Low	2013	78	587	68	38	17	44
Y03	5	1910	ABCO	Flat	Mod.	2013	67	382	63	45	18	39
Y09	5	2370	ABMA	Flat	None	-	77	1330	121	34	12	51
Y12	6	2200	ABMA	Mod.	Low	2006	48	237	60	57	23	44
Y14	6	2380	ABCO	Flat	Mod.	2010	30	127	38	61	27	48
D02	6	2190	ABCO	Steep	None	-	63	632	55	33	15	33
Y04	7	1640	ABCO	Mod.	Mod.	2013	66	343	73	52	21	50
Y05	7	1570	ABCO	Steep	High	2013	49	82	38	77	29	61
Y10	7	2390	ABMA	Mod.	None	-	68	539	114	51	17	62
D03	7	2160	ABCO	Steep	None	-	69	311	98	63	22	51
D05	7	2600	ABMA	Flat	None	-	57	547	107	49	19	44
Y06	8	1840	ABMA	Steep	Mod.	2009	52	142	58	72	27	57
Y08	8	2020	ABMA	Mod.	Low	2013	52	130	52	71	25	55

Table 4 Results for individual tree detection.

Plot	Structure Class	Omission (%)	Commission (%)	*F*-score
Y07	2	38	28	0.65
D04	3	59	6	0.56
Y11	4	47	50	0.52
Y13	4	57	71	0.40
D01	4	36	12	0.73
Y01	5	54	43	0.48
Y02	5	41	46	0.58
Y03	5	41	56	0.55
Y09	5	77	25	0.31
Y12	6	49	56	0.49
Y14	6	53	53	0.47
D02	6	63	6	0.52
Y04	7	75	39	0.31
Y05	7	52	343	0.19
Y10	7	78	29	0.29
D03	7	56	37	0.49
D05	7	70	24	0.39
Y06	8	39	111	0.45
Y08	8	42	191	0.33

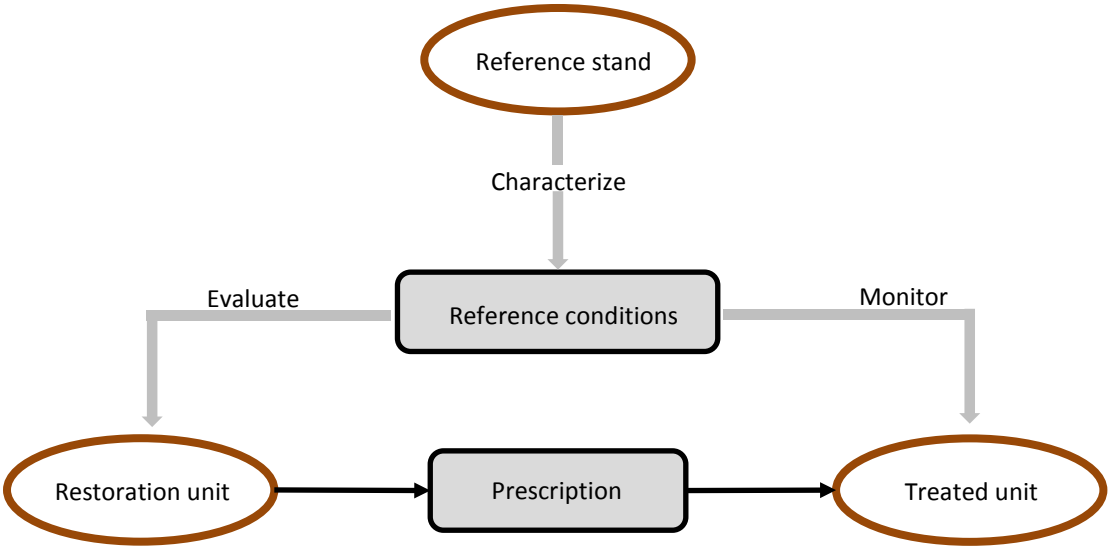

Figure 1 Framework for silvicultural restoration. The structure of a functionally intact reference stand is characterized, resulting in a quantitative reference condition dataset. The reference conditions are used to evaluate the current conditions of a restoration unit, informing development of the treatment prescription. After implementation, the treatment is monitored; this includes another round of comparison against reference conditions to evaluate progress toward structural goals. Characterization of reference conditions, evaluation of current conditions, and monitoring of the treated stand all require some ability to accurate quantify and compare forest structure.

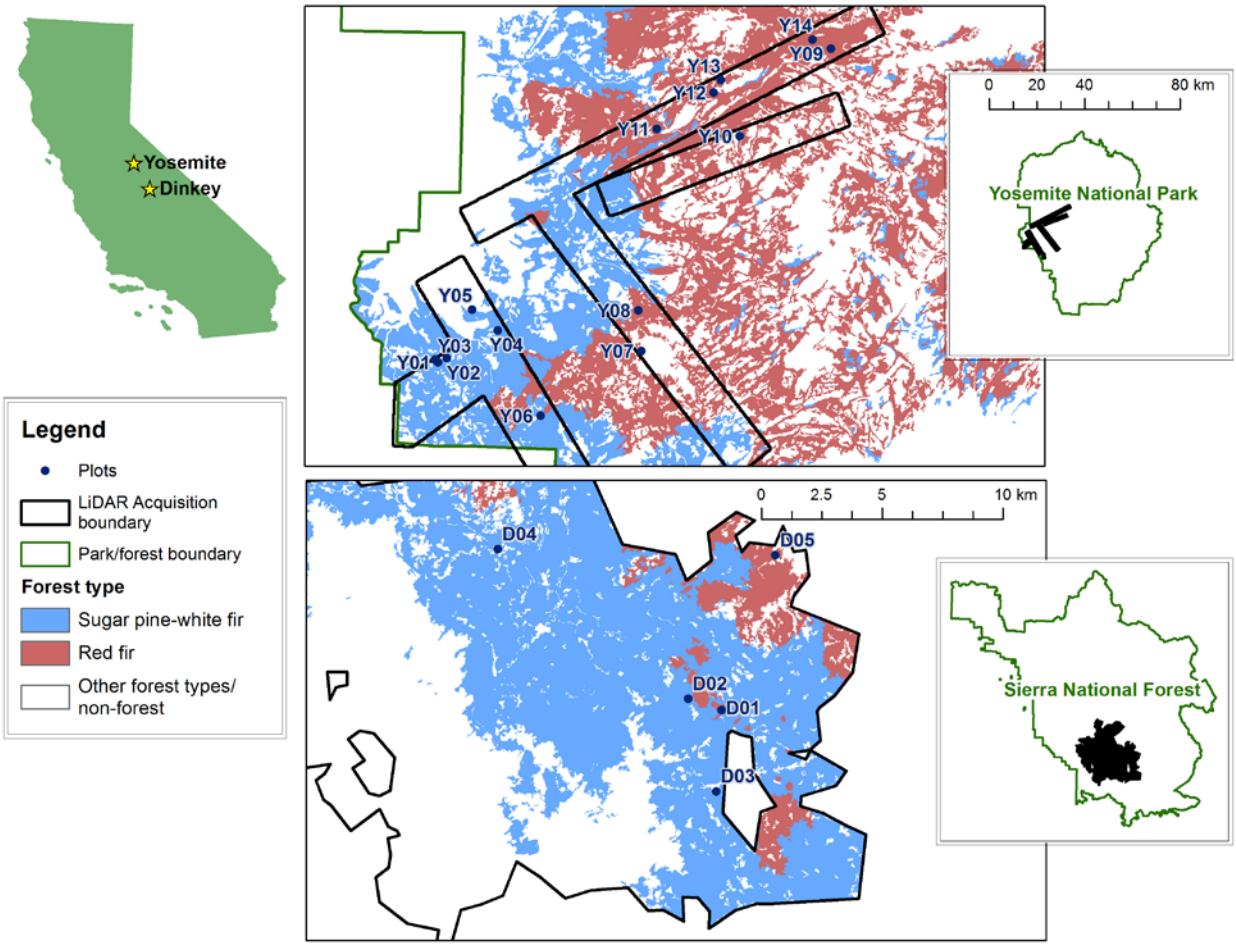

Figure 2 Yosemite and Dinkey study areas within the state of California, showing locations of LiDAR acquisition boundaries, forest types, and stem map plots.

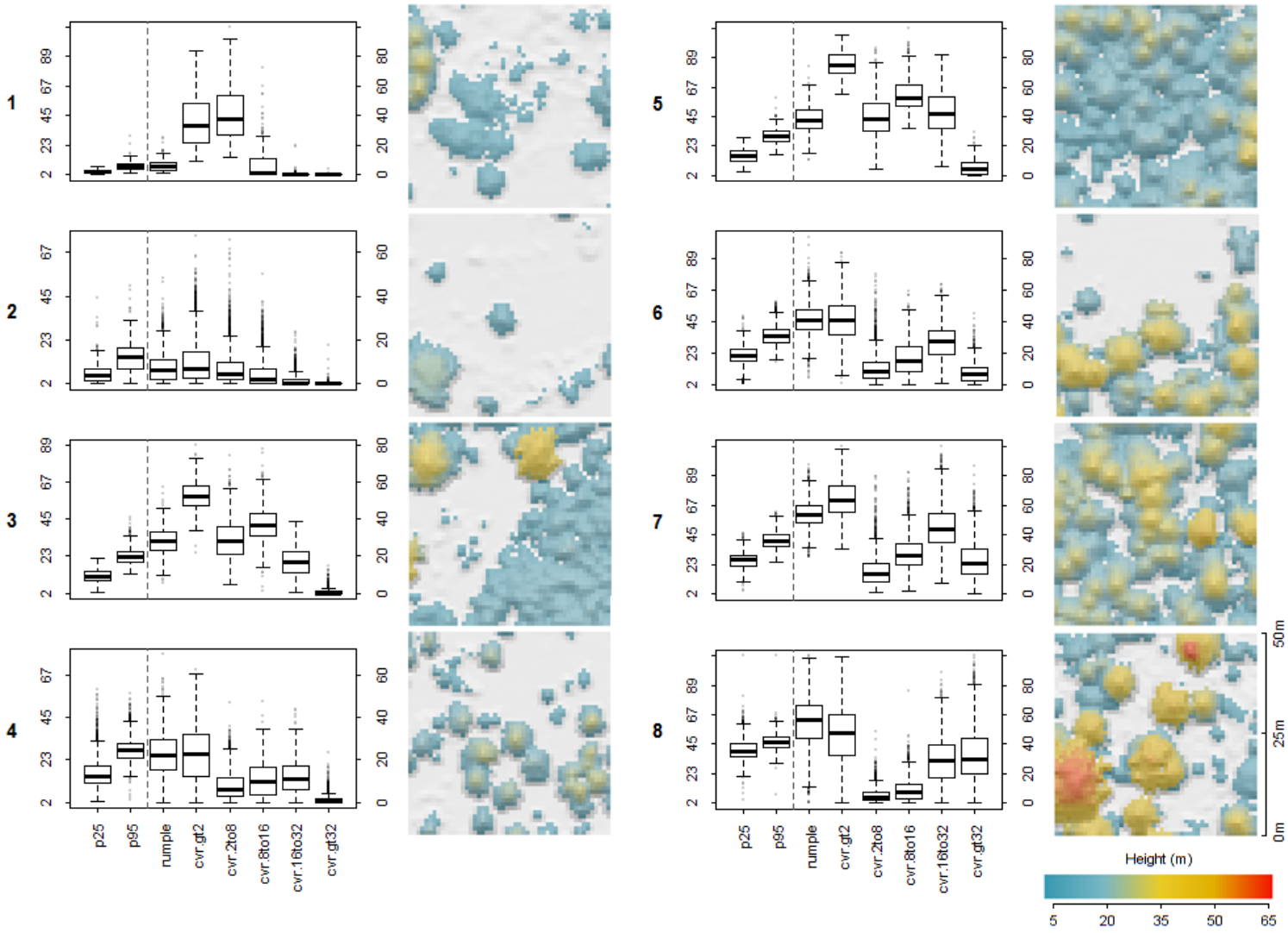

Figure 3 Overview of structure class characteristics. Boxplots show ranges of values within each structure class, while images are an overhead view of exemplar locations for each class. The dashed vertical line denotes the separation between the left-hand and right-hand scales: boxes left of the line correspond to the left axis (meters height), while boxes to the right of the line correspond to the right axis (percent). Classes are arranged in order of increasing 95th percentile height.

Boxplot codes: p25 = 25th percentile of LiDAR return heights; p95 = 95th percentile of LiDAR return heights; rumple = ratio of canopy surface area to ground area (rugosity); cvr.gt2 = total canopy cover above 2 m; cvr.2to8 = canopy cover in the stratum layer between 2 and 8 meters above the ground; cvr.8to16 = canopy cover 8 to 16 m; cvr.16to32 = canopy cover 16 to 32 m; cvr.gt32 = canopy cover above 32 m.

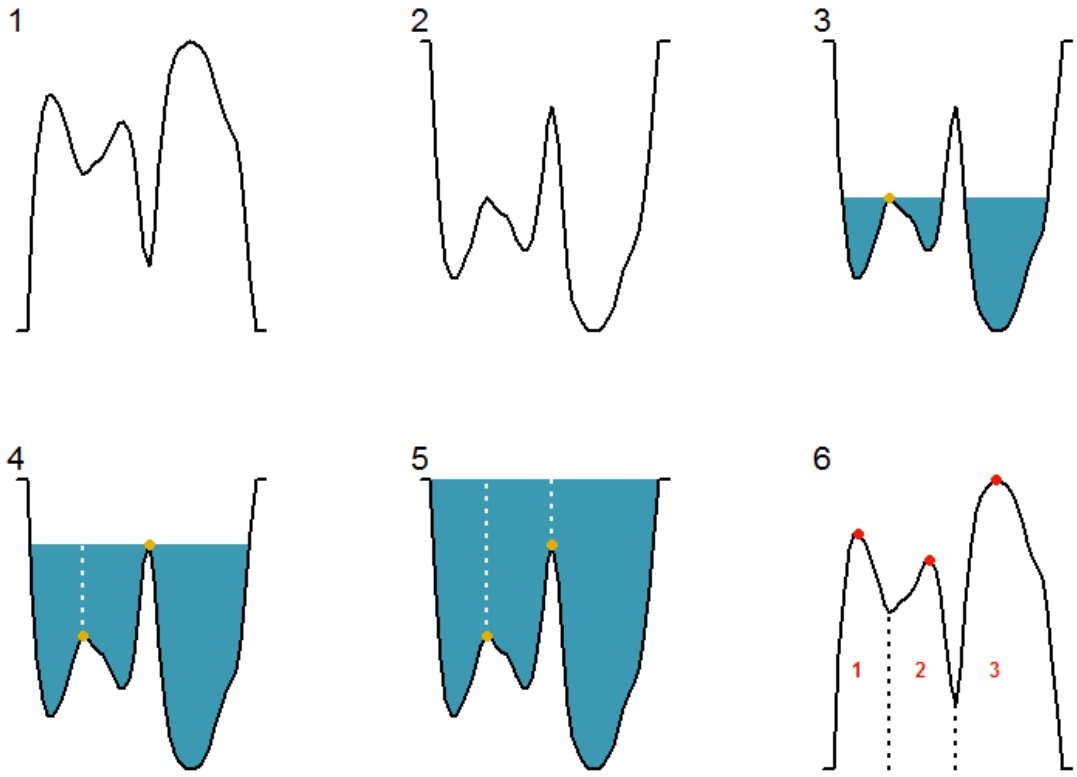

Figure 4 Overview of the watershed segmentation algorithm, presented here as a 2D concept, but actually performed in 3D. (1) The canopy surface model is draped over the LiDAR point cloud. (2) The canopy surface model is inverted. (3-5) The surface is imagined to be made of a permeable material, and is slowly lowered into water. Any time two separate pools come into contact (green points), a dam (white dashed lines) is formed. (6) The canopy surface model is righted. The dams are taken to be region boundaries, and high points within each region so defined are taken to be the treetops (red points).

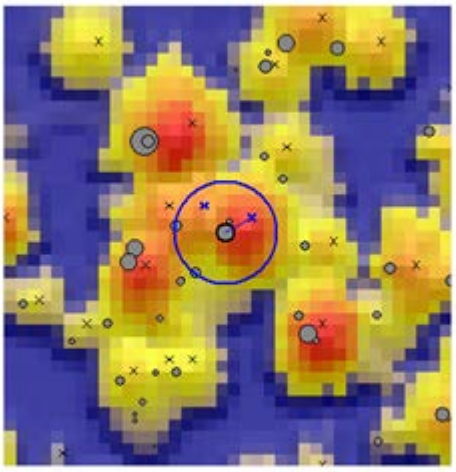

Figure 5 Method for associating identified segment maxima with plotted trees, from Vauhkonen et al. (2012). The tree of interest (bold grey circle) is buffered by its estimated canopy radius (blue circle). Any canopy maxima falling in this buffer are considered candidates (blue ×s). The 3D coordinates of each of the maxima are compared to that of the estimated treetop, and the nearest one is considered a match (thin blue line).

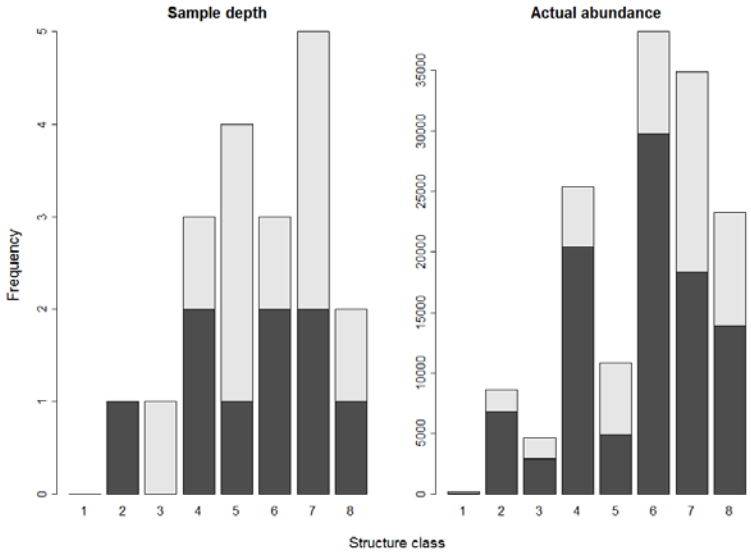

Figure 6 Results of sample stratification across structure classes by forest type. Actual abundance refers to the total abundance of classes across Yosemite and Dinkey LiDAR acquisitions. The sample *n* of 19 plots effectively covers the range of structural conditions across the study area.

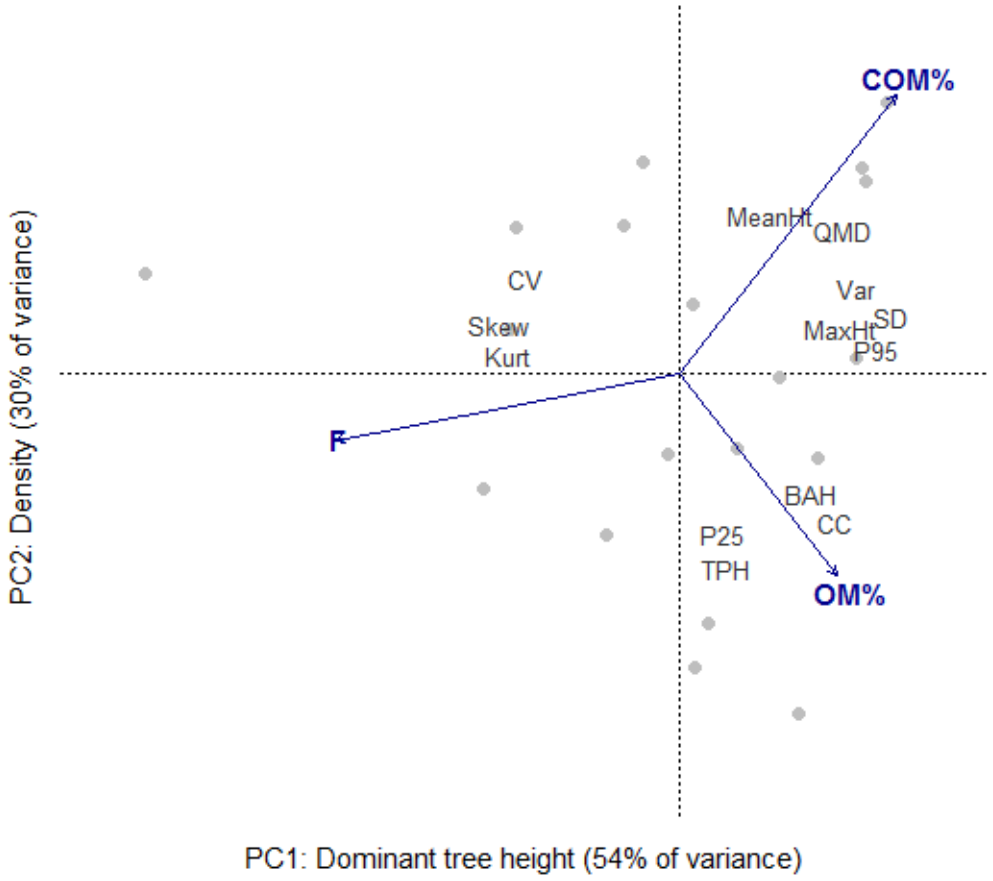

Figure 7 First two principal components (PCs) of ordinated plot-level structural metrics overlaid with fitted vectors of individual tree detection evaluation metrics. Grey dots are individual plots in PC-space. Dark grey text represents the variables that were ordinated on; location of the text in relation to the origin represents the highest gradient of change for that variable. Dark blue text and arrows follow the same concept, but for fitted evaluation metrics. Abbreviations: OM% = error rate of omission, COM% = error rate of commission, F = *F*-score. For definitions of structural metric abbreviations see 0.

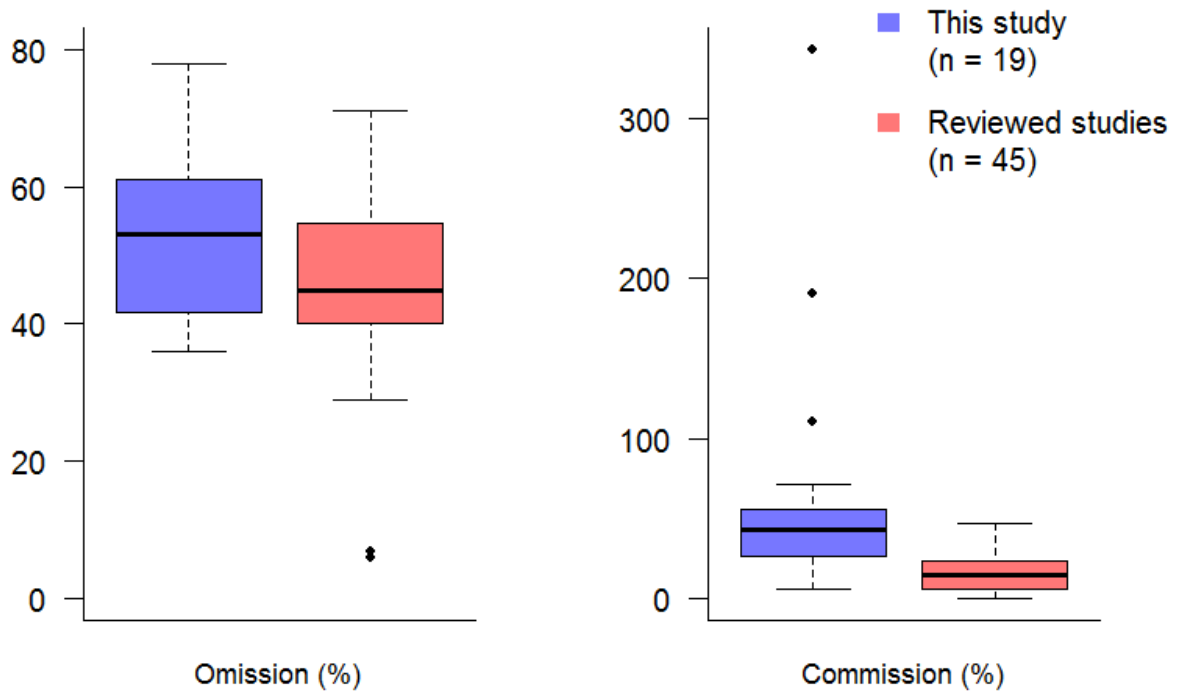

Figure 8 Individual tree detection accuracy metrics for this study compared to the same metrics for a review of 58 published studies. Error rates for this study are probably higher due to the greater complexity of individual tree and stand structure in the forests I assessed compared to many reviewed studies. In addition, it should be noted that this comparison is not direct, since different studies have employed evaluation criteria with varying levels of rigor.

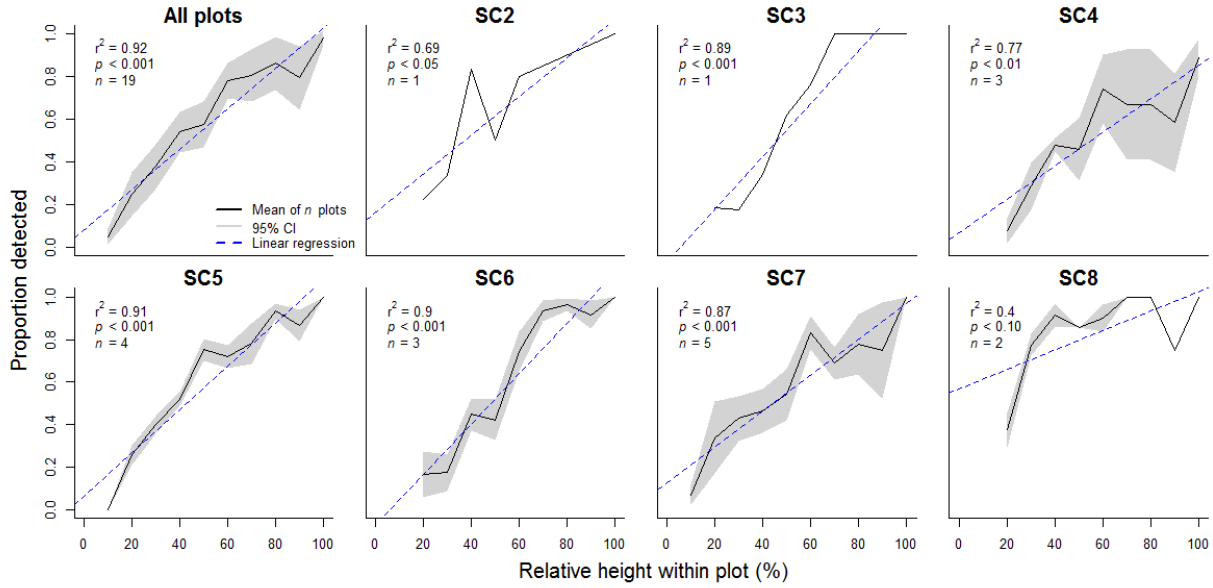

Figure 9 Detection rate by relative tree height aggregated over my 19 sample plots (first panel) and split out by the 7 sampled structure classes (remaining panels). To normalize between different plots, heights are expressed as percentages of the maximum tree height at each plot. Values on the *y*-axis are calculated on the basis of 10% bins. Detection rate increases quite linearly with relative tree height, a result that is consistent with many past studies (e.g., Vaukonen et al. 2012; Jakubowski et al. 2013).

Appendix A Regression models for total height, height to live crown, and crown spread

For each tree measured I recorded the following data: species, DBH (to the nearest 0.25 cm), vigor (classified as vigorous, declining, nearly dead, or snag), estimated age class (young, <100 years old; mature, 100-150; old, 150-250; or very old, >250), canopy stratum (emergent, dominant, co-dominant, intermediate, or understory), presence of various crown conditions (broken top, dead top, crown fork, bole fork, or reiterated top), and lean condition (angle from vertical in 5° increments and azimuth of lean to the nearest 1°). I also took more detailed measurements on a subset of trees: for a random 10% of the live trees in each plot, with a minimum of 5 trees, I additionally recorded total tree height (height), height to live crown (HLC), and average radial crown spread (crown spread).

I tested DBH, vigor, age class, canopy stratum, and crown conditions as predictor variables and settled on the following models:

$$\log(Height) \cong -0.34 + 0.84 * \log(DBH) + c_{spc1}, \quad \text{(A1)}$$

$$HLC \cong 4.68 + 0.08 * DBH + c_{spc2} + c_{crown}, \text{ and} \quad \text{(A2)}$$

$$CrownSpread \cong 0.98 + 0.04 * DBH + c_{spc3}. \quad \text{(A3)}$$

where:

$$c_{spc1} = \begin{cases} 0.19, Species = \text{ABCO} \\ 0.17, Species = \text{ABMA} \\ 0.00, Species = \text{CADE} \\ 0.15, Species = \text{PICO} \\ 0.18, Species = \text{PILA} \\ -0.06, Species = \text{PIJE or PIPO} \end{cases},$$

$$c_{spc2} = \begin{cases} 0.63, Species = \text{ABCO} \\ 1.90, Species = \text{ABMA} \\ 0.00, Species = \text{CADE} \\ -1.50, Species = \text{PICO} \\ 4.84, Species = \text{PILA} \\ -0.65, Species = \text{PIJE or PIPO} \end{cases},$$

$$c_{crown} = \begin{cases} 2.86, CrownClass = \text{E} \\ 0.68, CrownClass = \text{D} \\ 0.00, CrownClass = \text{C} \\ -1.08, CrownClass = \text{I} \\ -3.75, CrownClass = \text{U} \end{cases}, \text{ and}$$

$$c_{spc3} = \begin{cases} 0.12, Species = \text{ABCO} \\ -0.19, Species = \text{ABMA} \\ 0.00, Species = \text{CADE} \\ 0.16, Species = \text{PICO} \\ 1.30, Species = \text{PILA} \\ -0.58, Species = \text{PIJE or PIPO} \end{cases}.$$

Species codes are as follows: ABCO = *Abies concolor*, ABMA = *Abies magnifica*, CADE = *Calocedrus decurrens*, PICO = *Pinus contorta*, PILA = *Pinus lambertiana*, PIJE = *Pinus jeffreyi*,

PIPO = *Pinus ponderosa*. Crown class codes are as follows: E = emergent, D = dominant, C = codominant, I = intermediate, U = understory.

For the height regression, $r^2 = 0.86$, $p < 0.001$. For the HLC regression, $r^2 = 0.56$, $p < 0.001$. For the crown spread regression, $r^2 = 0.73$, $p < 0.001$.

I did not have enough measurements of hardwoods to include them in my models. Instead, I used the following published regression models (Larsen & Hann 1987 for *Quercus kelloggii*; Staudhammer & LeMay 2000 for *Alnus rubra*, as a surrogate for *Alnus rhombifolia*).
For *Quercus kelloggii*:

$$Height \cong \frac{4.5+\exp\left(b_1+b_2*DBH^{b_3}+b_4*BA\right)}{3.2808}, \qquad \text{(A4)}$$

where $b_1 = 4.63362$, $b_2 = -3.17216$, $b_3 = -0.411021$, $b_4 = 0.00198936$, and $BA = DBH^2 * 0.0008454$.

For *Alnus rhombifolia*:

$$Height \cong 1.3 + E1 * [1 - \exp(E2 * DBH^{E3})], \qquad \text{(A5)}$$

where $E1 = 26.5495$, $E2 = -0.03079$, and $E3 = 1.20438$.

In all cases, the units of height, HLC, and crown spread are m, while the units of DBH are cm.

References

Larsen, D.R. & D.W. Hann. 1987. Height-diameter equations for seventeen tree species in Southwest Oregon. Forest Research Lab, Oregon State University College of Forestry, Corvallis, OR.

Staudhammer, C. & V. LeMay. 2000. Height prediction equations using diameter and stand density measures. *Forestry Chronicle* **76(2)**: 303-309.

Appendix B Choice of CSM creation and preprocessing parameters

Introduction

Most LiDAR individual tree detection (ITD) methods require tuning to achieve optimal results. Tuning is comprised of (1) creating the LiDAR data source(s), (2) preprocessing the LiDAR data sources, (3) choosing values for mechanistic parameters, and (4) choosing values for heuristic parameters. Any of these steps may be omitted for a particular ITD approach, and it is rare that all four are necessary for any given approach.

All ITD methods work from some fine-scale LiDAR data product. In the vast majority of cases, this is either a canopy surface model (CSM) or the LiDAR point cloud itself, although other products (e.g., Delanauy triangulation of the first-return points; Alexander 2009) are occasionally used. These data can be created and preprocessed in different ways, which can have various effects on ITD performance. For example, CSMs can be created at varying resolutions, while point clouds can be created from only first returns versus all returns. Either of these data sources can then be filtered in some way to remove noise and enhance features.

Mechanistic parameters are those which represent a physical measure that can be determined on the ground and has a known mode of influencing the ITD algorithm. For example, local maxima (LM) methods require a crown width parameter which can be held constant or estimated based on an allometric relationship with tree height (Pitkanen et al. 2004; Popescu & Wynne 2004), while object-matching methods require knowledge of crown shape (e.g., paraboloid, conoid, ellipsoid) (Persson et al. 2002; Tittman et al. 2011).

In contrast, heuristic parameters do not necessarily represent or correspond with any ground-based measurements, and their influence on performance of the ITD algorithm is not usually well-known, although it may follow a predictable pattern. For example, some ITD techniques rely on an α value (Tittman et al. 2011), which does not represent a particular measureable dimension of a tree or forest. Because heuristic parameters cannot be estimated based on measured data, they must be arrived at through trial and error.

Tuning ITD algorithms requires some data that are not contained within the LiDAR acquisition. In particular, selecting values for mechanistic parameters requires some individual tree measurements or forest inventory data, while choosing methods to create and preprocess the LiDAR data source and selecting values for heuristic parameters requires some "truth" dataset to test against for trial and error analyses. Usually, this means that plots must be installed on the ground to provide the truth data.

The tuning process becomes problematic when working with large and heterogeneous landscapes. As forest conditions vary over space, so do the optimal choices for ITD tuning. To adequately tune across variable landscapes requires having truth data for the variety of conditions that occur. The time and expense required to gather these data can be prohibitive.

In this report, I use the 19 plots described in the main study to develop a basis for tuning two ITD methods based on metrics that can be calculated from LiDAR data. As a result of this work, future users of LiDAR data in the Sierra Nevada should be able to tune these ITD methods without the need to install plots themselves.

Methods

I carried out my analysis using two ITD methods: the watershed transform (Vincent & Soille 1991) and the local maxima (LM) method (Hyyppa et al. 2001). Both of these methods are commonly used and freely available. The watershed transform does not have any parameters *per*

se, while the LM method has one mechanistic parameter: the allometric relationship between tree height and crown spread. Both methods operate from the CSM and are strongly influenced by CSM creation and preprocessing methods.

I satisfied the mechanistic parameter of the LM method using measured heights and crown spreads from my plots, manifest in the following equation:

$$CrownSpread = 1.5546 + 0.1949 * Height \qquad \text{(B1)}$$

I tuned the CSM creation and preprocessing parameters using a brute force approach: I selected several values across the reasonable range of each parameter, then tried every reasonable combination of these. The parameters I varied were CSM resolution, smoothing type, and smoothing window size (Figure B1). All CSMs had a lower threshold of 2 m to remove understory vegetation (Figure B2). I tested a total of 74 combinations, which are given in Table B1.

For each of the 74 combinations on each plot, I performed both ITD methods. To perform the watershed transform, I used TreeSeg, a prototype tool being developed for the Fusion LiDAR Toolkit (http://forsys.cfr.washington.edu/fusion.html). For the LM method, I used CanopyMaxima, which is currently available in the Fusion LiDAR Toolkit.

I evaluated my results using the same methods presented in the main study, namely, by associating mapped trees to LiDAR-identified trees using methods from Vauhkonen et al. (2012) and then calculating the *F*-score. The *F*-score integrates errors of omission and commission, ranging from 0 (poor) to 1 (perfect).

To explore patterns in parameters versus accuracy, I mapped the *F*-score as a function of CSM parameters. In my preliminary analyses, I observed that sites with higher density had different response characteristics than sites with lower density. But density cannot be measured by LiDAR, and so is not useful for developing LiDAR-based tuning recommendations. Instead, I used canopy cover (CC), which is related to density but can be measured by LiDAR, as a basis for grouping sites. I split my sites into three CC groups using standard break points: low (<30%), medium (30-70%), and high (>70%). For each group, I constructed a 3-dimensional surface with the *x*-axis representing CSM resolution, the *y*-axis representing smoothing window size, and the *z*-axis representing the mean *F*-score. I chose not to separate out data by smooth type, since doing so made visualization more difficult and did not provide additional insight. I visualized each surface by plotting the level set of the *z*-axis on the *xy*-plane.

Results and Discussion

In terms of overall accuracy, the watershed method outperformed the LM method (Figure B3; Table B2), with median *F*-scores of 0.48 and 0.31, respectively. However, the patterns of error were quite different between the two methods: the watershed method had a lower rate of omission errors (0.53 compared to 0.77), while the LM method had a lower commission error rate (0.05 compared to 0.43). This is probably because the LM method features an exclusionary zone around each identified maximum point. The procedure identifies the tallest trees first, and then works downward, guaranteeing that the dominant trees have no neighbors within their estimated crown radius. However, it is not necessarily the case that the crown spread of one tree excludes all other trees; on the contrary, clumping of trees is to be expected (Larson & Churchill 2008). The LM method only detects the dominant tree within a given area – even when more than one of the trees clumped in the area has a well-differentiated apex – resulting in elevated omission rates and diminished commission rates. On the balance it appears that this phenomenon is a detriment, since the *F*-scores for the LM method are significantly lower ($p < 0.001$, paired

Student's *t*-test) than for the watershed method. Because the watershed method seems to be better suited for my purposes, I did not complete the tuning analysis with the LM method.

Segmentation accuracy followed a relatively predictable pattern in relation to CSM resolution and smoothing window size. Optimal choices of CSM resolution and smoothing window tended toward large pixel sizes and small smoothing windows for plots with lower CC, and small pixel sizes with medium smoothing windows under higher CC (Figure B4). Large smoothing windows (9 pixels and greater) never yielded optimal results, and unsmoothed CSMs were only preferable in combination with larger pixels (2 m or greater) at low CC. The middle range of parameters – CSM resolution of 0.5-1 m and smoothing window of 3-5 pixels – performed reasonably well across all densities.

As a guide for implementation, I provide the following recommendations. For low CC sites (<30%), I suggest creating CSMs of 1-2 m resolution and no smoothing. For sites with moderate canopy cover (30-70%), I suggest CSMs of 0.5-1 m resolution with a 5×5 or 3×3 smoothing window. For sites above 70% CC, I recommend using either a 0.5 m CSM with a 3×3 smoothing window or a 0.25 m CSM with a 5×5 smoothing window. In any event, it is prudent to tend to larger pixel sizes/smaller smoothing windows when CC is lower, and smaller pixel sizes/larger smoothing windows when CC is higher.

As a compromise, a 0.75 m CSM with a 3×3 smoothing window should provide adequate results for all but the highest and lowest density sites, where results will be under- and oversegmented, respectively. If the distribution of CC across the area in question is platykurtic (i.e., both very high and very low CC are not rare), it may be better to tend toward a larger pixel size/smaller smoothing window solution than in the average case, so that more of the errors are errors of omission rather than errors of commission. This is preferable because errors of omission are more readily dealt with than errors of commission. In particular, it is simpler to draw inferences from connected blocks of canopy that may represent more than one individual tree (undersegmentation) than from small slices of canopy that represent fractional trees (oversegmentation).

I did not find any patterns between relative successes of different smooth types, except that the difference between not smoothing and smoothing is substantial. Using some sort of smoothing proved beneficial for all but the densest sites. I recommend using a mean smooth in most instances, since it is typically the quickest and easiest filter to apply.

Among different plots, there was little consistency in terms of which CSMs yielded the highest *F*-scores (Table B2). However, applying the CC-based tuning criteria yielded results in the upper quartile of plot-wise *F*-score distributions in all but one case (Figure B5). In fact, using a single "compromise" CSM for all plots yielded similar results, with only two sites below the 75^{th} percentile *F*-score. This indicates that one or a few choices of CSM can provide good enough ITD performance across a variety of structural conditions on the landscape level. To the extent that my sample sites represent mid-elevation Sierra Nevada forests, my CSM construction recommendations can be applied across large areas in this region without additional tuning.

References

Alexander, C. 2009. Delineating tree crowns from airborne laser scanning point cloud data using Delaunay triangulation. *International Journal of Remote Sensing* **30(14)**: 3843-3848.

Larson, A.J. & D.J. Churchill. 2012. Tree spatial patterns in fire-frequent forests of western North America, including mechanisms of pattern formation and implications for designing fuel reduction and restoration treatments. *Forest Ecology and Management* **267**: 74-92.

Persson, Å., J. Holmgren, and U. Söderman. 2002. Detecting and Measuring Individual Trees Using an Airborne Laser Scanner. *Photogrammetric Engineering & Remote Sensing* **68(9)**: 925-932.

Pitkänen, J., M. Maltamo, J. Hyyppä, and X. Yu. 2004. Adaptive methods for individual tree detection on airborne laser based canopy height model. *International Archives of Photogrammetry, Remote Sensing, and Spatial Information Sciences* **36**: 187-191.

Popescu, S.C. & R.H. Wynne. 2004. Seeing the Trees in the Forest: Using Lidar and Multispectral Data Fusion with Local Filtering and Variable Window Size for Estimating Tree Height. *Photogrammetric Engineering & Remote Sensing* **70(5)**: 589-604.

Tittmann, P., S. Shafii, B. Hartsough, and B. Hamann. 2011. Tree Detection and Delineation from LiDAR point clouds using RANSAC. SilviLaser 2011 Proceedings.

Vauhkonen, J., L. Ene, S. Gupta, J. Heinzel, J. Holmgren, J. Pitkänen, S. Solberg, Y. Wang, H. Weinacker, K.M. Hauglin, V. Lien, P. Packalén, T. Gobakken, B. Koch, E. Næsset, T. Tokola, and M. Maltamo. 2012. Comparative testing of single-tree detection algorithms under different types of forest. *Forestry* **85(1)**: 27-40.

Vincent, L. & P. Soille. 1991. Watersheds in Digital Spaces: An Efficient Algorithm Based on Immersion Simulations. *IEEE Transactions on Pattern Analysis and Machine Intelligence* **13(6)**: 583-598.

Table B1 Tested combinations of canopy surface model resolution and smooth window. Very large smooth windows were not tested on the larger cell sizes. For each of these 23 combinations, I tested mean, median, and Gaussian smooth types. Additionally, I tested an unsmoothed version for each CSM resolution, for a total of 74 unique parameterizations.

		CSM Resolutions (m)				
		0.25	**0.5**	**1.0**	**2.0**	**3.0**
Smooth Windows (pixels)	**3**	×	×	×	×	×
	5	×	×	×	×	×
	7			×	×	×
	9	×	×			
	13	×	×			
	17	×	×			
	21	×	×			
	25	×	×			

Table B2 Results for watershed and local maxima individual tree detection methods. Resolution, smooth type, and smooth window columns give the highest-ranked (according to the *F*-score) CSM preprocessing parameters for each plot. Omission rate, Commission rate, and *F*-score columns give the associated evaluation metrics.

	Watershed						Local maxima					
Plot	Res. (m)	Smooth type	Smooth win. (px)	Om. rate	Com. rate	F-score	Res. (m)	Smooth type	Smooth win. (px)	Om. rate	Com. rate	F-score
D01	0.25	gaussian	9	0.24	0.20	0.78	0.25	mean	3	0.42	0.06	0.71
D02	0.25	mean	5	0.35	0.52	0.60	0.25	median	13	0.60	0.31	0.47
D03	0.25	median	9	0.51	0.25	0.56	0.25	none	-	0.62	0.29	0.46
D04	0.5	none	-	0.22	0.38	0.72	0.25	median	9	0.61	0.11	0.52
D05	0.5	none	-	0.44	0.56	0.53	0.25	median	9	0.63	0.45	0.40
Y01	0.5	none	-	0.28	0.84	0.56	0.25	median	13	0.73	0.07	0.40
Y02	0.5	gaussian	3	0.38	0.49	0.59	0.25	median	9	0.63	0.17	0.48
Y03	1	none	-	0.51	0.17	0.59	0.25	median	5	0.47	0.29	0.59
Y04	0.25	median	5	0.58	0.61	0.42	0.25	mean	9	0.78	0.16	0.32
Y05	1	mean	3	0.67	0.76	0.32	0.25	gaussian	17	0.43	0.57	0.53
Y06	1	mean	5	0.61	0.24	0.48	0.25	gaussian	3	0.47	0.50	0.52
Y07	1	none	-	0.38	0.28	0.65	0.25	none	-	0.92	0.04	0.14
Y08	1	median	3	0.67	0.15	0.45	0.25	mean	9	0.55	0.42	0.48
Y09	0.25	gaussian	5	0.48	0.72	0.46	0.25	median	3	0.76	0.19	0.33
Y10	0.5	none	-	0.62	0.27	0.46	0.25	mean	5	0.80	0.06	0.31
Y11	0.5	mean	3	0.47	0.50	0.52	0.25	gaussian	3	0.57	0.25	0.51
Y12	0.25	median	9	0.43	0.36	0.59	0.25	gaussian	5	0.48	0.13	0.63
Y13	0.5	mean	9	0.52	0.14	0.59	0.25	mean	13	0.52	0.05	0.63
Y14	1	gaussian	3	0.53	0.38	0.51	0.25	gaussian	17	0.59	0.13	0.53

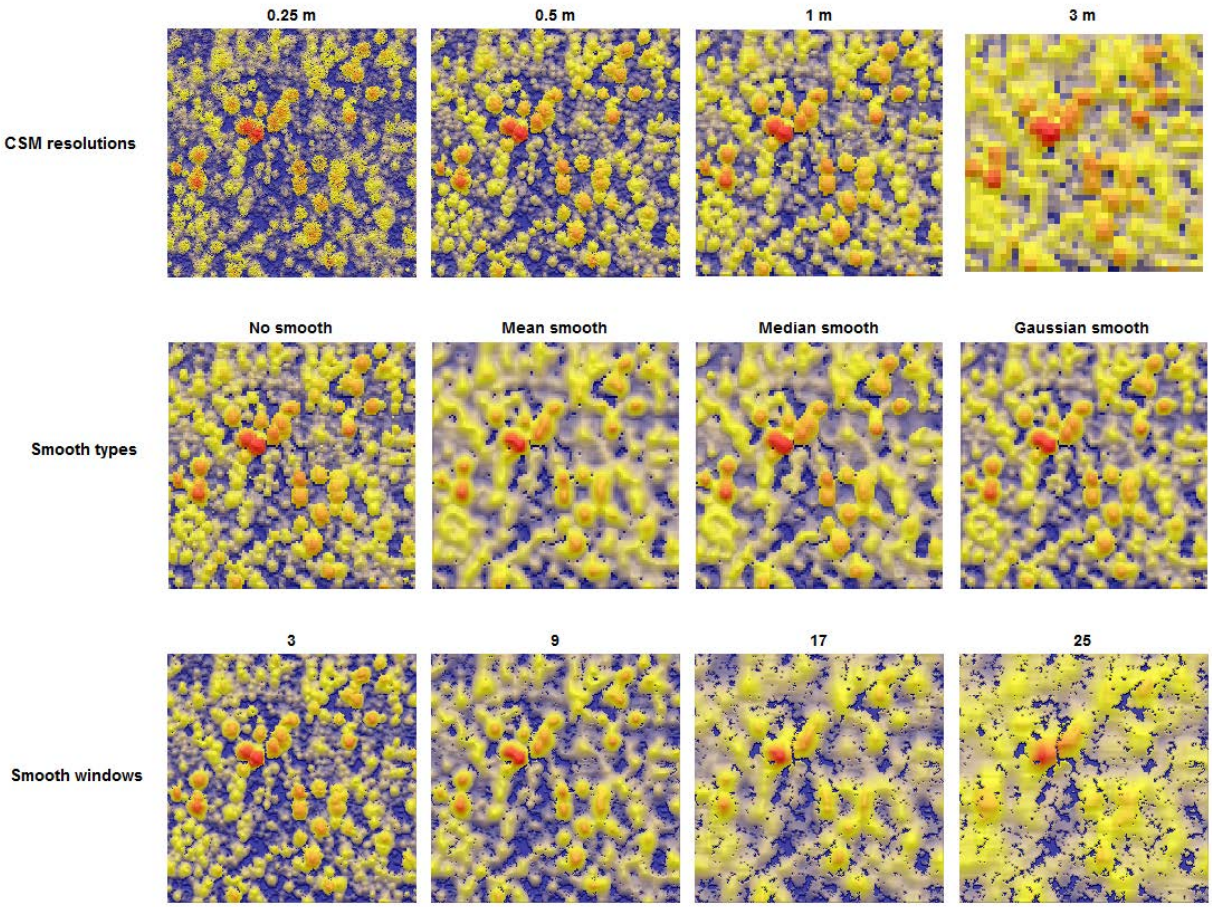

Figure B1 Examples of canopy surface models (CSMs) preprocessed using different parameters. For the CSM resolutions, the same point cloud is sampled at different pixel resolutions. For the Smooth types, each unsmoothed CSM is processed using three different types of smoothing. For the Smooth windows, the same smooth type is performed with many different focal windows. These examples are provided to illustrate the results of different preprocessing methods; a list of all factorial combinations of these methods can be found in Table B1.

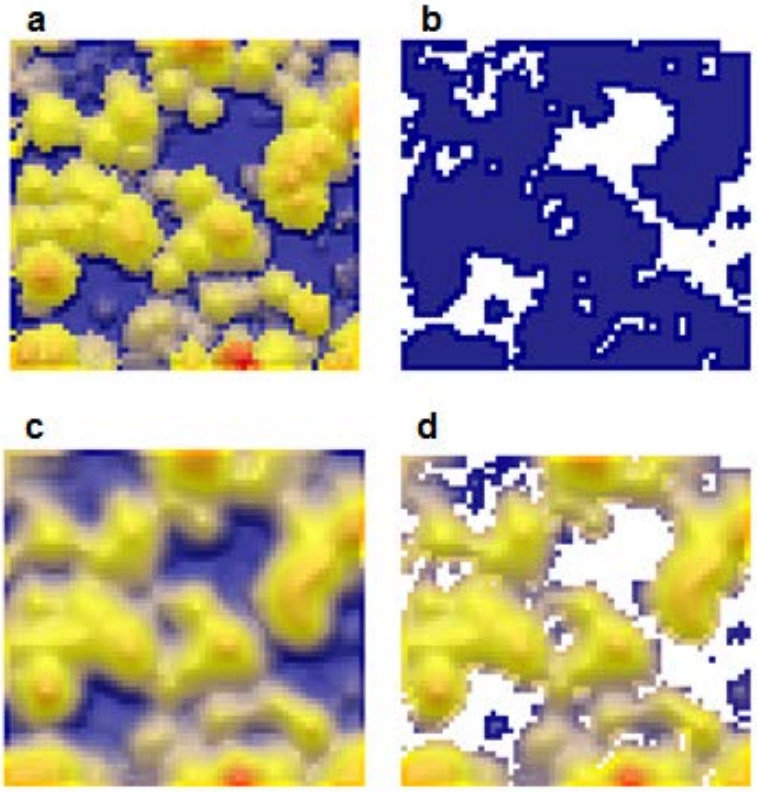

Figure B2 Demonstration of the method for thresholding canopy surface models (CSMs). First, the raw, unsmoothed CSM (a) is thresholded at 2 m height to create a binary canopy/no canopy mask layer (b). Then, this mask is applied to all smoothed CSMs (c), resulting in the final smoothed and thresholded version (d). This preserves the higher fidelity canopy presence data, which would be lost if the thresholding were applied to (c) directly.

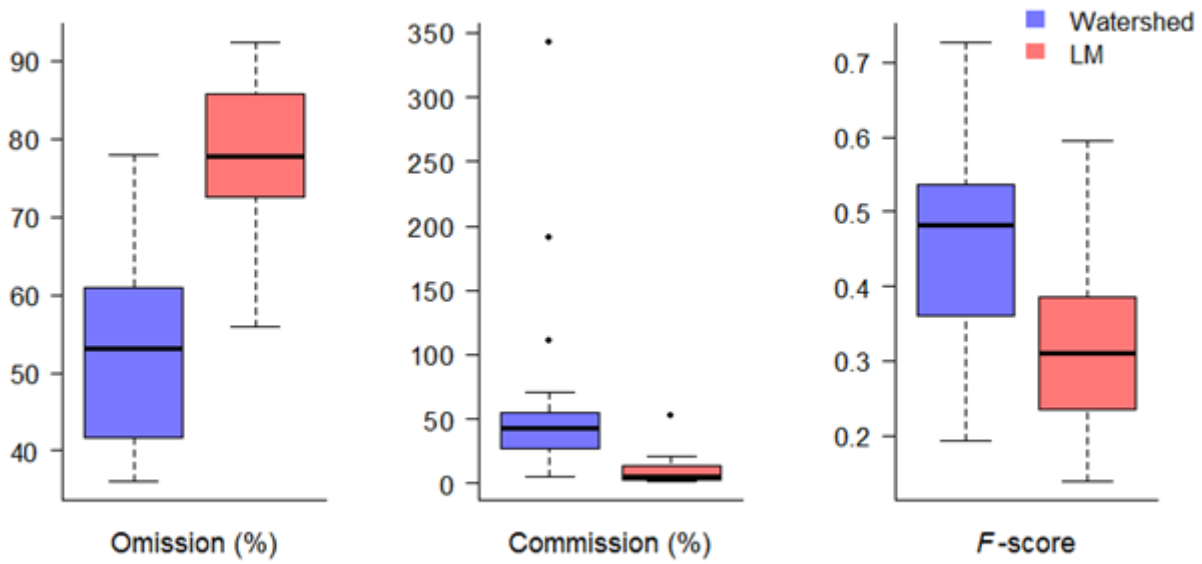

Figure B3 Comparison between watershed and local maxima (LM) ITD method accuracy on 19 plots.

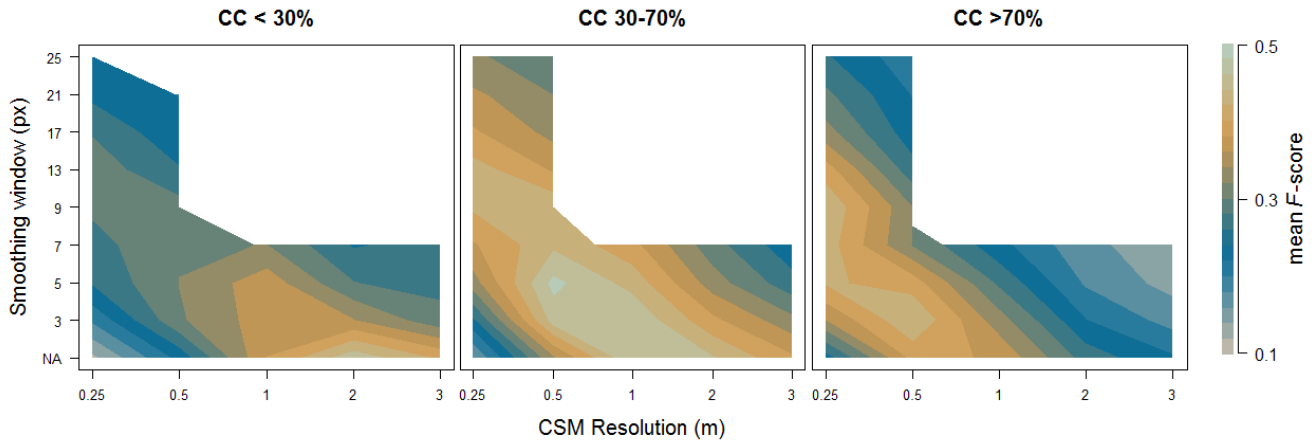

Figure B4 Level set of 3-dimensional surface showing response of ITD accuracy to CSM creation and preprocessing parameters. Panels are stratified by canopy cover (CC). Higher *F*-scores indicate more accurate segmentation. In more open plots, larger pixel sizes and smaller smoothing windows produce the best results. For more closed plots, the best parameters have smaller pixel sizes with moderate smoothing windows. These results can be used to select CSM creation methods for any forests within the range of variation of this study area.

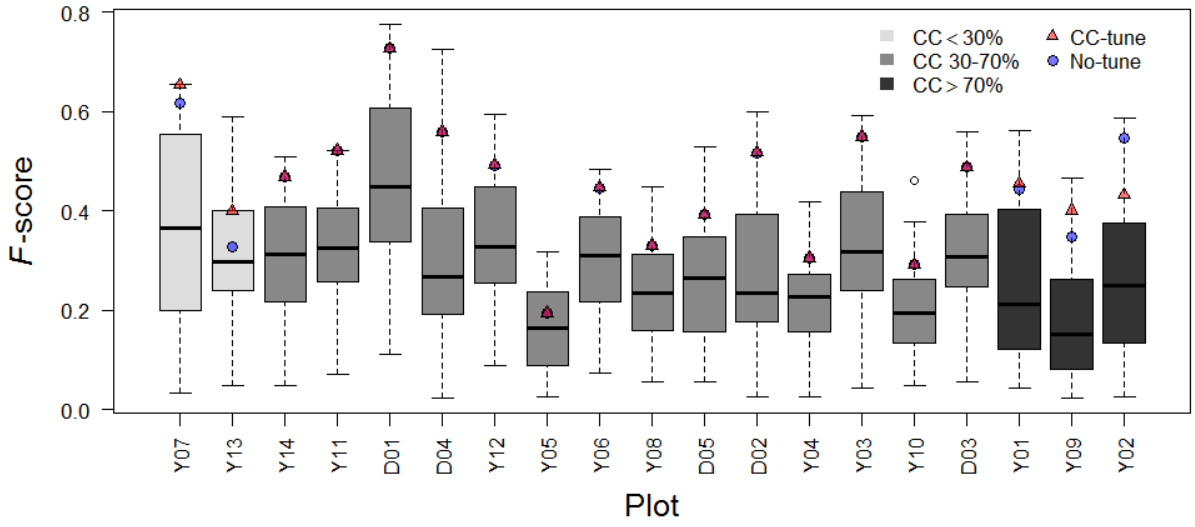

Figure B5 Results of tuning compared to range of segmentation results for each plot. Box and whisker plots give the ranges and quartiles of *F*-scores for all 74 CSM permutations, and are colored according to the plots' canopy cover classes. The high end of the whiskers represents the "best" results achieved by any of the tested CSMs. Small colored boxes represent the results as tuned by canopy cover classes (red) or by flat tuning as a compromise for all plots (blue).

CC-tune parameters: CC < 30%: 1 m CSM resolution, no smoothing; CC 30-70%: 0.5 m CSM resolution, 3×3 mean smooth; CC >70%: 0.25 m CSM resolution, 5×5 mean smooth. *No-tune parameters*: 0.5 m CSM resolution, 3×3 mean smooth.

Appendix C Review of individual tree segmentation methods

Methods included were those which reported at least one of detection, commission, or omission rates.

* = watershed segmentation method
† = local maxima method

Study	Method name (if multiple)	Locale	Forest type	Detection	Commission	Omission
Alexander 2009		Finland	Pine-spruce-birch	0.63	0.04	0.41
Barilotti et al. 2009		Italy	Spruce-fir-beech	0.925		
Breidenbach et al. 2010		Norway	Spruce-pine-birch	0.55	0.2	0.06
Chen et al. 2006*†		California	Oak savanna	0.65		
Edson & Wing 2011*†		Oregon	Douglas-fir - grand fir	0.59		
Falkowski et al. 2008†		Idaho	Douglas-fir - grand fir - western red-cedar - western larch		0.06	0.43
Heurich et al. 2004		Germany	Spruce-fir-birch	0.442	0.054	
Holmgren & Persson 2004		Sweden	Spruce-pine-birch	0.71		
Huang et al. 2009*†		China	Oak-pine			0.65
Kaartinen et al. 2012†	Definiens	Finland	Pine-spruce-birch	0.3	0.006	0.68
Kaartinen et al. 2012*	FGI-LOCM	Finland	Pine-spruce-birch	0.75	0.181	0.4
Kaartinen et al. 2012*	FGI-MCV	Finland	Pine-spruce-birch	1.05	0.388	0.35
Kaartinen et al. 2012*	FGI-MLOG	Finland	Pine-spruce-birch	0.7	0.149	0.42
Kaartinen et al. 2012†	FGI-VWS	Finland	Pine-spruce-birch	0.6	0.061	0.45
Kaartinen et al. 2012	FOI	Finland	Pine-spruce-birch	0.55	0.05	0.5
Kaartinen et al. 2012*	Hannover	Finland	Pine-spruce-birch	0.25	0	0.71
Kaartinen et al. 2012*	Metla	Finland	Pine-spruce-birch	0.65	0.061	0.45
Kaartinen et al. 2012	Norwegian	Finland	Pine-spruce-birch	0.85	0.233	0.45
Kaartinen et al. 2012†	Texas	Finland	Pine-spruce-birch	0.35	0.003	0.6
Kaartinen et al. 2012	Udine	Finland	Pine-spruce-birch	0.9	0.265	0.4
Koukoulas & Blackburn 2005		England	Deciduous	0.6		

Li et al. 2012		California	Sierra Nevada mixed conifer	0.86	0.04	
Persson et al. 2002		Sweden	Spruce-pine-birch	0.71	0.002	0.29
Reitberger et al. 2007*		Germany	Spruce-beech	0.74	0.05	
Schardt et al. 2002*		Austria	Spruce-pine-oak	0.5	0.05	0.45
Stumberg et al. 2014		Norway	Spruce-pine-birch tundra	0.45		
Tao et al. 2014		California	Sierra Nevada mixed conifer	0.91		
Tompalski et al. 2014		Germany	Spruce	0.901	0.029	0.068
Vauhkonen et al. 2012†	1	Germany	Oak-beech-birch	0.52	0.233	0.601
Vauhkonen et al. 2012†	1	Germany	Scots pine	0.926	0.282	0.334
Vauhkonen et al. 2012†	1	Sweden	Pine-spruce-birch	0.776	0.296	0.453
Vauhkonen et al. 2012†	1	Norway	Pine-spruce-birch	0.494	0.23	0.619
Vauhkonen et al. 2012	2	Germany	Oak-beech-birch	0.876	0.473	0.538
Vauhkonen et al. 2012	2	Germany	Scots pine	0.789	0.343	0.482
Vauhkonen et al. 2012	2	Sweden	Pine-spruce-birch	0.651	0.228	0.497
Vauhkonen et al. 2012	2	Norway	Pine-spruce-birch	0.513	0.3	0.641
Vauhkonen et al. 2012*	3	Germany	Oak-beech-birch	0.46	0.121	0.596
Vauhkonen et al. 2012*	3	Germany	Scots pine	0.532	0.094	0.518
Vauhkonen et al. 2012*	3	Sweden	Pine-spruce-birch	0.689	0.144	0.41
Vauhkonen et al. 2012*	3	Norway	Pine-spruce-birch	0.528	0.166	0.559
Vauhkonen et al. 2012	4	Brazil	Eucalyptus plantation	0.639		
Vauhkonen et al. 2012	4	Germany	Oak-beech-birch	0.927	0.395	0.439
Vauhkonen et al. 2012	4	Germany	Scots pine	1.114	0.393	0.324
Vauhkonen et al. 2012	4	Sweden	Pine-spruce-birch	0.716	0.103	0.357
Vauhkonen et al. 2012	4	Norway	Pine-spruce-birch	0.568	0.204	0.548
Vauhkonen et al. 2012	5	Brazil	Eucalyptus plantation	0.932		
Vauhkonen et al. 2012	5	Germany	Oak-beech-birch	0.816	0.297	0.427
Vauhkonen et al. 2012	5	Germany	Scots pine	0.783	0.167	0.348
Vauhkonen et al. 2012	5	Sweden	Pine-spruce-birch	0.858	0.191	0.306
Vauhkonen et al. 2012	5	Norway	Pine-spruce-birch	0.681	0.254	0.492
Vauhkonen et al. 2012	6	Brazil	Eucalyptus plantation	0.9		

Vauhkonen et al. 2012	6	Germany	Oak-beech-birch	0.654	0.185	0.467
Vauhkonen et al. 2012	6	Germany	Scots pine	0.652	0.097	0.411
Vauhkonen et al. 2012	6	Sweden	Pine-spruce-birch	0.685	0.069	0.362
Vauhkonen et al. 2012	6	Norway	Pine-spruce-birch	0.452	0.139	0.611
Yao et al. 2012		Germany	Spruce-beech	0.6	0.09	
Yu et al. 2011*		Finland	Pine-spruce	0.69		
Zhao et al. 2014*		China	Spruce-pine-juniper	0.39		

References

Alexander, C. 2009. Delineating tree crowns from airborne laser scanning point cloud data using Delaunay triangulation. *International Journal of Remote Sensing* **30(14)**: 3843-3848.

Barilotti, A., F. Crosilla, and F. Sepic. 2009. Curvature analysis of LiDAR data for single tree species classification in alpine latitude forests. *IAPRS Laser scanning* **38(3)**: 129-134.

Breidenbach, J., E. Næsset, V. Lien, T. Gobakken, and S. Solberg. 2010. Prediction of species specific forest inventory attributes using a nonparametric semi-individual tree crown approach based on fused airborne laser scanning and multispectral data. *Remote Sensing of Environment* **114**: 911-924.

Chen, Q., D. Baldocchi, P. Gong, and M. Kelly. 2006. Isolating Individual Trees in a Savanna Woodland Using Small Footprint Lidar Data. *Photogrammetric Engineering & Remote Sensing* **72(8)**: 923-932.

Edson, C. & M.G. Wing. 2011. Airborne Light Detection and Ranging (LiDAR) for Individual Tree Stem Location, Height, and Biomass Measurements. *Remote Sensing* **3**: 2494-2528.

Falkowski, M.J., A.M.S. Smith, P. Gessler, A.T. Hudak, and L.A. Vierling. 2008. The influence of conifer forest canopy cover on the accuracy of two individual tree measurement algorithms using lidar data. *Canadian Journal of Remote Sensing* **34S2**: S1-S13.

Heurich, M., Å. Persson, J. Holmgren, and E. Kennel. 2004. Detecting and measuring individual trees with laser scanning in mixed mountain forest of Central Europe using an algorithm developed for Swedish boreal forest conditions.*International Archives of Photogrammetry, Remote Sensing, and Spatial Information Sciences* **36**: 307-312.

Holmgren, J. & Å Persson. 2004. Identifying species of individual trees using airborne laser scanner. *Remote Sensing of Environment* **90**: 415-423.

Kaartinen, H., J. Hyyppä, X. Yu, M. Vastaranta, H. Hyyppä, A. Kukko, M. Holopainen, C. Heipke, M. Hirschmugl, F. Morsdorf, E. Næsset, J. Pitkänen, S. Popescu, S. Solberg, B.M. Wolf, and J.-C. Wu. 2012. An International Comparison of Individual Tree Detection and Extraction Using Airborne Laser Scanning. *Remote Sensing* **4**: 950-974.

Koukoulas, S. & G.A. Blackburn. 2005. Mapping individual tree location, height and species in broadleaved deciduous forest using airborne LIDAR and multi-spectral remotely sensed data. *International Journal of Remote Sensing* **26(3)**: 431-455.

Li, W., Q. Guo, M.K. Jakubowski, and M. Kelly. 2012. A New Method for Segmenting Individual Trees from the Lidar Point Cloud. *Photogrammetric Engineering & Remote Sensing* **78(1)**: 75-84.

Persson, Å., J. Holmgren, and U. Söderman. 2002. Detecting and Measuring Individual Trees Using an Airborne Laser Scanner. *Photogrammetric Engineering & Remote Sensing* **68(9)**: 925-932.

Reitberger, J., M. Heurich, P. Krzystek, and U. Stilla. 2007. Single Tree Detection in Forest Areas with High-density LiDAR Data. *International Archives of Photogrammetry, Remote Sensing, and Spatial Information Sciences* **26**: 139-144.

Schardt, M., M. Zielger, A. Wimmer, R. Wack, and J. Hyyppä. 2002. Assessment of Forest Parameters by Means of Laser Scanning. *International Archives of Photogrammetry, Remote Sensing, and Spatial Information Sciences* **34(3/A)**: 302-309.

Stumberg, N., O.M. Bollandsås, T. Gobakken, and E. Næsset. 2014. Automatic Detection of Small Single Trees in the Forest-Tundra Ecotone Using Airborne Laser Scanning. *Remote Sensing* **6**: 10152-10170.

Tao, S., Q. Guo, L. Li, B. Xue, M. Kelly, W. Li, G. Xu, and Y. Su. 2014. Airborne Lidar-derived volume metrics for aboveground biomass estimation: A comparative assessment for conifer stands. *Agricultural and Forest Meteorology* **199**: 24-32.

Tompalski, P., P. Wężyk, M. Weidenbach, R. de Kok, and P. Hawryło. 2014. A comparison of LiDAR and image-derived canopy height models for individual tree crown segmentation with object based image analysis. *South-Eastern European Journal of Earth Observation and Geomatics* **3(2S)**: 4 pp.

Vauhkonen, J., L. Ene, S. Gupta, J. Heinzel, J. Holmgren, J. Pitkänen, S. Solberg, Y. Wang, H. Weinacker, K.M. Hauglin, V. Lien, P. Packalén, T. Gobakken, B. Koch, E. Næsset, T. Tokola, and M. Maltamo. 2012. Comparative testing of single-tree detection algorithms under different types of forest. *Forestry* **85(1)**: 27-40.

Yao, W., P. Krzytek, and M. Heurich. 2012. Tree species classification and estimation of stem volume and DBH based on single tree extraction by exploiting airborne full-waveform LiDAR data. *Remote Sensing of Environment* **123**: 368-380.

Yu, X., J. Hyyppä, M. Vastaranta, M. Holopainen, and R. Viitala. 2011. Predicting individual tree attributes from airborne laser point clouds based on the random forests technique. *ISPRS Journal of Photogrammetry & Remote Sensing* **66**: 28-37.

Zhao, D., Y. Pang, Z. Li, and L. Liu. 2014. Isolating individual trees in a closed coniferous forest using small footprint lidar data. *International Journal of Remote Sensing* **35(20)**: 7199-7218.